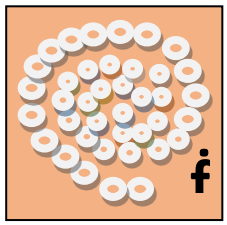

International Journal of Mathematical Analysis and Modelling

(Formerly Journal of the Nigerian Society for Mathematical Biology)

Volume 8 Issue 2, 2025

ISSN (Print): 2682 - 5694
ISSN (Online): 2682 – 5708
www.tnsmb.org

Mathematical modelling of the endemic phase of Covid-19 infection considering vaccination breakthrough, revaccination and reinfection

F.C. Eze*, K.O. Idowu†, U.M. Adam‡, and D.O. Olofin§

Abstract

The transition of COVID-19 from a pandemic to an endemic phase requires a better understanding of its long-term dynamics, especially regarding vaccination breakthroughs, reinfection, and revaccination. This study develops and analyzes a deterministic mathematical model to quantify the endemic dynamics of COVID-19, using New York, USA, as a case study. The model takes into account vaccination, vaccine breakthrough infections, revaccination of previously immunized individuals, and reinfection. The well-posedness of the model is established by demonstrating the non-negativity of solutions and identifying an invariant region. The disease-free equilibrium (DFE) is derived, and its basic reproduction number (R_0) is computed using the next-generation matrix. Local stability of the DFE is confirmed through the Jacobian matrix, while global stability of both the DFE and the endemic equilibrium is proven using suitably constructed Lyapunov functions. A sensitivity analysis of (R_0) indicates that the contact rate among non-vaccinated individuals (β_c) and the asymptomatic transmission modification factor (η_A) are the most significant parameters, with positive sensitivity indices of 0.987 and 0.518, respectively. In contrast, the recovery rate for symptomatic individuals (γ_2) and the vaccination rate (θ) showed substantial negative effects. Numerical simulations, conducted in Python, quantified the endemic equilibrium, revealing stable patterns across population compartments and a notably lower force of infection among vaccinated individuals. Scenarios that examined varying contact rates (β_c) demonstrated a direct, linear relationship with the force of infection. Additionally, a three-dimensional analysis of vaccine coverage and efficacy revealed a compensatory relationship, illustrating the herd immunity threshold. Importantly, the revaccination rate emerged as a critical control parameter, with increases from 0.1 to 0.3 day^{-1} correlating with a 40-60% reduction in peak infections and a 50-70% decrease in hospitalizations. The findings indicate that the endemic persistence of COVID-19 is highly sensitive to contact rates within the unvaccinated population and the infectiousness of asymptomatic cases. The results support the need for targeted interventions, such as ongoing vaccination and revaccination campaigns, rather than broad, uniform measures, to keep the epidemic below critical thresholds and effectively manage the burden on healthcare systems. This study provides a quantitative framework for public health policy in the endemic phase of COVID-19.

Keywords and phrases: vaccination breakthrough; revaccination; reinfection; asymptomatic; and symptomatic infection

1 Introduction

The COVID-19 pandemic, triggered by the new SARS-CoV-2 virus, has profoundly affected public health and economic systems around the world since it surfaced in late 2019. With the rapid development and widespread availability of vaccines, the severity of COVID-19-related diseases and mortality

*Corresponding Author; Department of Mathematics & Statistics, Federal Polytechnic Nekede, Owerri, Nigeria; E-mail:ezefrankline86@gmail.com

†Department of Mathematics, Purdue University, West Lafayette, Indiana 47907, USA; E-mail: kidowu@purdue.edu

‡Department of Mathematics,Durham University,Durham, United Kingdom; E-mail: uadam@dunelm.org.uk

§Department of Mathematical Sciences, Georgia Southern University, Statesboro, 30458, US; E-mail: do05368@georgiasouthern.edu.

has decreased significantly, especially in countries with high vaccination rates [1]. As a result, in May 2023, the World Health Organization (WHO) announced that COVID-19 no longer qualifies as a Public Health Emergency of International Concern [2]. However, the virus continues to circulate throughout the world, with recurring waves fueled by diminished immunity, the emergence of new variants, and breakthrough infections, thus ensuring its continued importance as a public health issue [3]. Although vaccination continues to be the most effective method for reducing COVID-19 transmission and severity, the immunity developed through vaccination is not infallible. Increasing reports of breakthrough infections—where vaccinated individuals still contract the virus—are attributed to diminished vaccine effectiveness against new variants and the natural waning of immunity over time [4]. At the same time, reinfections, or cases of infection in those who have previously recovered, are rising, especially with variants such as Omicron and its sub-lineages [5]. At the same time, cases of reinfection—where individuals who have previously recovered from an infection experience it again—are now well-documented. These reinfections occur more frequently when immunity decreases or when individuals come into contact with variants that are antigenically different [6, 7]. These developments underscore the limitations of assuming lifelong immunity and highlight the need for updated modeling approaches that take these complexities into account.

Although COVID-19 vaccinations provide significant protection, the rise of reinfections and breakthrough infections among vaccinated individuals is becoming a major concern worldwide [8]. No vaccine offers complete immunity, which makes breakthrough cases of COVID-19 a foreseeable issue [9, 10, 11]. This implies that even fully vaccinated individuals (those who have received three doses of the COVID-19 vaccine) can still become infected with the virus. Breakthrough infections and reinfections are not unique to COVID-19; they can occur with various other diseases as well. A breakthrough infection is defined as the detection of SARS-CoV-2 RNA or antigens in a respiratory sample taken from a person at least 14 days after completing all recommended doses of a COVID-19 vaccine authorized by the Food and Drug Administration [12]. RNA viruses mutate at a rate significantly higher than that of their hosts, sometimes up to a million times faster [13]. However, the incidence of COVID-19 vaccine breakthroughs has been reported to be relatively low [13], although this rate might be more pronounced in larger vaccinated populations. Additionally, the emergence of viral variants, such as Delta and Omicron, could elevate the likelihood of breakthrough infections [14, 15]. According to a report by Heather that 46,312 cases of SARS-CoV-2 breakthrough infections were identified across 13 jurisdictions in the USA, with 80% (2,976) of hospitalizations and 90% (616) of deaths occurring in fully vaccinated individuals [16]. Similarly, several cohort studies involving healthcare workers have indicated that the probability of testing positive for SARS-CoV-2 post-vaccination is higher than the risk observed during initial vaccine clinical trials [17, 18].These developments raise critical questions regarding the durability of immunity, the effectiveness of booster campaigns, and the long-term trajectory of COVID-19 as an endemic disease. As immunity—both natural and vaccine-induced—is neither permanent nor fully protective, breakthrough cases and reinfections have become important drivers of ongoing transmission [19]. They also present challenges for public health strategies that rely on long-lasting immunity to achieve population-level protection. Therefore, developing a mathematical model is essential to enhance our understanding of COVID-19 transmission dynamics in the population, taking into account variables such as reinfection and vaccine breakthroughs.

Mathematical models have played a crucial role in analyzing the spread of COVID-19 and evaluating the potential effects of interventions like vaccination, social distancing, and quarantine [20, 21, 22, 23, 24, 25]. Nevertheless, several early models failed to consider the potential for breakthrough infections and reinfections [26, 27, 28]. As the virus shifts from a pandemic to an endemic phase, it is vital to update these models to incorporate realistic immunological dynamics that align with contemporary epidemiological trends. Fractional-order models and delay differential equations were utilized to more effectively represent memory effects and latency in immune responses [26, 27, 28]. These models highlighted that overlooking the possibility of reinfection may result in an underestimation of future cases, particularly in populations with high density or low vaccination coverage. [22] introduced a fractional-order model that accounted for both vaccine breakthrough and reinfection, illustrating the

long-term consequences of imperfect immunity. Their findings emphasized the importance of sustained monitoring and booster vaccinations, even in communities with a high initial rate of vaccine uptake. In this research, we create a compartmental model to analyze the transmission dynamics of COVID-19, specifically factoring in vaccination breakthroughs and reinfections in a post-pandemic setting. The model categorizes the population into compartments of susceptible, vaccinated, exposed, infectious, recovered, and reinfected individuals, while also considering waning immunity and the partial protection offered by vaccines. Utilizing both analytical and numerical methods, we explore the conditions under which COVID-19 continues to thrive or diminishes, and we evaluate the long-term implications of breakthrough infections and reinfections on disease dynamics. The findings from this model are intended to guide ongoing public health initiatives, particularly in relation to booster vaccination strategies and long-term surveillance.
This study differentiates itself from existing works by addressing several important gaps that this research aims to explore:

- **Incorporation of Revaccination Dynamics:** This study differs from most current COVID-19 endemic models by incorporating the revaccination of individuals who have already been immunized. The model examines the impact of booster doses on long-term infection dynamics and herd immunity in an endemic context.
- **Breakthrough Infections and Reinfection:** The model incorporates both vaccine breakthrough infections (infections occurring despite vaccination) and reinfections (infections following recovery). This dual inclusion offers a more accurate and comprehensive representation of COVID-19 transmission in a partially immune population.
- **Endemic-Phase Framework (Post-Pandemic Modeling):** Most earlier models concentrated on pandemic or temporary phases; this model is specifically designed to measure the ongoing presence of COVID-19. It offers insights into the long-term equilibrium behavior of the disease amid ongoing transmission, vaccination efforts, and decreasing immunity.
- **Empirical Application to New York, USA:** The study utilizes New York's epidemiological data to parameterize the model, providing a specific, data-driven case study that illustrates how the theoretical model can be applied to real-world management of endemic situations.

This model is unique as it combines revaccination, breakthrough infections, and reinfections within a single framework for endemic COVID-19. It supports its analysis with comprehensive mathematical proofs and offers quantitative insights for public health related to long-term epidemic control features that are usually not addressed together in a single study. Together, these contributions enhance the understanding of COVID-19 dynamics in the endemic phase in a relevant manner for policy.

2 Model descriptions

We consider a deterministic nine-compartmental human population model. The total population is divided into the epidemiological sub-classes, which are susceptible population (S), vaccinated individuals (V), exposed individuals (E), vaccinated exposed individuals (V_E), quarantine individuals (Q) asymptomatic infected individuals (A), infectious individuals (I), hospitalized individuals (H) and recovered individuals (R). The susceptible population is increased by the recruitment rate represented by Λ, while all the compartments are decreased by the natural mortality rate μ. Fraction of new recruits individuals are vaccinated against COVID-19 at the rate θ, while unsuccessful vaccinated individuals are returned to the susceptible population at the rate $(1-\theta)$. Susceptible individuals acquire the COVID-19 virus through contacts with asymptomatic infected individuals and infected individuals by a force of infection λ_c, while β_1 and β_2 denote the COVID-19 transmission probabilities per contact. The effective contact rate per unit time is represented by c, and ϵ represents the infection reduction of vaccinated individuals. We assumed that individuals leave the exposed class at rates α_1, α_2, and α_3. Vaccinated exposed (V_E)

individuals and exposed (E) individuals become quarantined at the rate π and α_1, respectively. Individuals who recovered naturally from COVID-19 while in the quarantine class are transferred back to the vaccinated class at a rate $\rho(1-\chi)$ for re-vaccination against future COVID-19. Individuals become infected (I) at the rate α_2, while individuals become asymptomatic infected (A) at the rate α_3. Asymptomatic infected individuals become infected (I) at the rate m, while the remaining portion recovers from the disease at the rate γ_1. The remaining individuals who developed symptoms of COVID-19 while in quarantine are moved to the infected class (I) at the rate $\rho\chi$.

Chronically infected individuals are hospitalized at a rate ψ while the remaining individuals are recovered at a rate γ_2. Individuals in the infected and hospitalized class die with COVID-19-induced death rate δ. We assumed that death due to COVID-19 are negligible at asymptomatic infected (A) class. Individuals at hospitalized class can recovered at a rate γ_3. Individuals who have recovered (R) from COVID-19 have probability of returning back to the Susceptible class at a rate ϕ due to loss of immunity.

2.1 Assumption of the model

1. We assume vaccinated exposed individual class
2. All individual class are decreased by the natural death rate.
3. There is currently no evidence that individuals develop permanent immunity against Covid-19.
4. The rate of disease transmission from asymptomatic individuals are less than that of infected and hospitalized individuals
5. The disease-induced death rate is negligible at asymptomatic infected class
6. Asymptomatic infected individuals and hospitalized individuals experiences additional disease-induce death rate.
7. Quarantine individuals who recovered naturally from COVID-19 while in quarantine are transferred back to vaccinated class at rate $\rho(1-x)$ for revaccination
8. Infected individuals can only be hospitalized or recovered from the disease. While hospitalized individuals can recovered or die off.

Table 1: Description of Variables

Variables	Descriptions
S	Susceptible Individuals
V	Vaccinated individuals
E	Exposed individuals
V_E	Vaccinated exposed individuals
Q	Quarantine individuals
A	Asymptomatic infected individuals
I	Infected (Symptomatic)Individuals
H	Hospitalized individuals
R	Recovery individuals

We consider a human population partitioned into the following compartments: susceptible individuals (S), vaccinated individuals (V), vaccinated–exposed individuals (V_E), exposed individuals (E), quarantined individuals (Q), infectious symptomatic (I), infectious asymptomatic (A), hospitalized individuals (H), and recovered individuals (R). The total population at time t is

$$N(t) = S(t) + V(t) + V_E(t) + E(t) + Q(t) + I(t) + A(t) + H(t) + R(t).$$

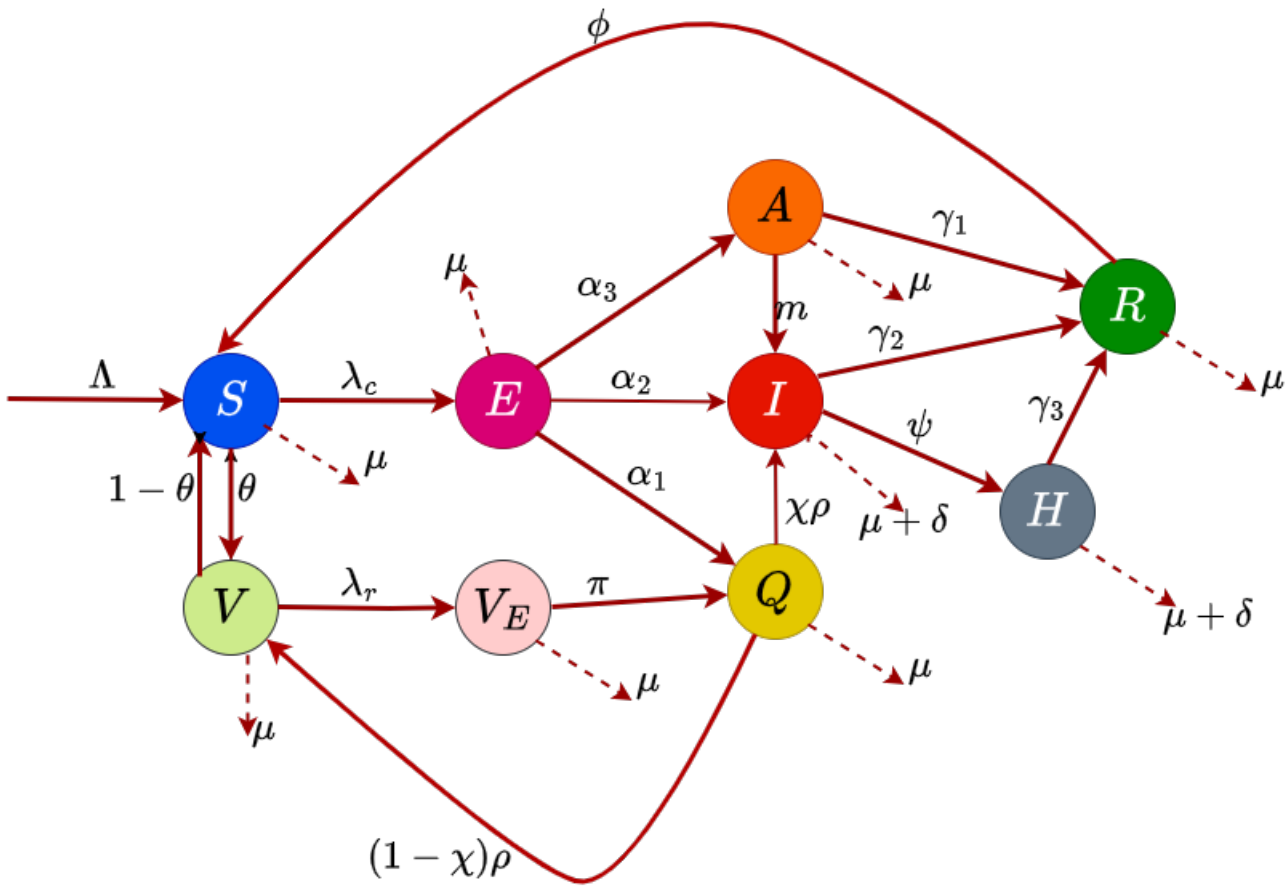

Figure 1: Model Diagram

Model equations

The transmission dynamics are governed by the following system of differential equations:

$$
\begin{aligned}
\frac{dS}{dt} &= (1-\theta)\Lambda + \phi R - \lambda_c S - \mu S,\\
\frac{dV}{dt} &= \theta\Lambda + (1-\chi)\rho Q - \lambda_r V - \mu V,\\
\frac{dV_E}{dt} &= \lambda_r V - \pi V_E - \mu V_E,\\
\frac{dE}{dt} &= \lambda_c S - (\alpha_1+\alpha_2+\alpha_3+\mu)E,\\
\frac{dQ}{dt} &= \alpha_1 E + \pi V_E - (\rho+\mu)Q,\\
\frac{dA}{dt} &= \alpha_3 E - (m+\gamma_1+\mu)A,\\
\frac{dI}{dt} &= \alpha_2 E + \chi\rho Q + mA - (\gamma_2+\psi+\mu+\delta)I,\\
\frac{dH}{dt} &= \psi I - (\gamma_3+\mu+\delta)H,\\
\frac{dR}{dt} &= \gamma_1 A + \gamma_2 I + \gamma_3 H - (\phi+\mu)R.
\end{aligned}
\tag{1}
$$

where,

$$\lambda_c(t) = \beta_c \frac{I(t) + \eta_A A(t) + \eta_H H(t)}{N(t)},$$

Table 2: Description of Parameters

Parameters	Descriptions
Λ	Recruitment (immigration) rate into the population.
θ	Fraction of new recruits vaccinated at entry.
μ	Natural death rate.
ϕ	Rate of waning immunity ($R \to S$).
β_c	Effective contact rate for COVID–19 transmission.
η_A	Modification parameter for infectiousness of asymptomatic individuals.
η_H	Modification parameter for infectiousness of hospitalized individuals.
β_r	Transmission parameter for the vaccinated individuals
α_1	Progression rate from exposed (E) to quarantine (Q).
α_2	Progression rate from exposed (E) to symptomatic infection (I).
α_3	Progression rate from exposed (E) to asymptomatic infection (A).
π	Rate at which vaccinated-exposed individuals (V_E) are quarantined.
ρ	Rate of leaving quarantine (Q).
χ	Proportion of quarantined individuals progressing to infectious (I).
$1-\chi$	Proportion of quarantined individuals returning to V for revaccination
m	Progression rate from asymptomatic infection (A) to symptomatic infection (I).
ψ	Hospitalization rate of symptomatic infectives ($I \to H$).
ε	is the vaccine efficacy, representing the fractional reduction in susceptibility due to vaccination.
γ_1	Recovery rate of asymptomatic individuals ($A \to R$).
γ_2	Recovery rate of symptomatic individuals ($I \to R$).
γ_3	Recovery rate of hospitalized individuals ($H \to R$).
δ	Disease-induced death rate (applies to I and H).

and

$$\lambda_r(t) = \beta_r(1-\varepsilon)\frac{I(t)+\eta_A A(t)+\eta_H H(t)}{N(t)}.$$

3 Model analysis

3.1 Non-negativity of the solutions

In order for model 1 to be epidemiologically meaningful, it is necessary to show that the solutions remain non-negative for all $t \geq 0$.

Theorem 3.1. *Assume the initial conditions*

$$S(0) \geq 0,\ V(0) \geq 0,\ E(0) \geq 0,\ V_E(0) \geq 0,\ Q(0) \geq 0,\ A(0) \geq 0,\ I(0) \geq 0,\ H(0) \geq 0,\ R(0) \geq 0.$$

Then the solution

$$\big(S(t), V(t), E(t), V_E(t), Q(t), A(t), I(t), H(t), R(t)\big)$$

of system 1 satisfies

$$S(t) \geq 0,\ V(t) \geq 0,\ E(t) \geq 0,\ V_E(t) \geq 0,\ Q(t) \geq 0,\ A(t) \geq 0,\ I(t) \geq 0,\ H(t) \geq 0,\ R(t) \geq 0$$

for all $t \geq 0$.

Proof. We write each equation of system 1 in a form suitable for the integrating factor method. For each compartment X we will show $X(t) \geq 0$ by deriving its integral representation.

From the first equation of (2.1),

$$\dot{S} = (1-\theta)\Lambda + \phi R - (\lambda_c + \mu)S.$$

Define $a_S(t) = \lambda_c(t) + \mu \geq 0$ and $b_S(t) = (1-\theta)\Lambda + \phi R(t) \geq 0$. The equation is

$$\dot{S} + a_S(t)S = b_S(t).$$

Multiplying by the integrating factor $\exp\big(\int_0^t a_S(s)\,ds\big)$ and integrating from 0 to t gives

$$S(t) = S(0)e^{-\int_0^t a_S(s)\,ds} + \int_0^t e^{-\int_s^t a_S(u)\,du} b_S(s)\,ds.$$

Since $S(0) \geq 0$, $a_S(\cdot) \geq 0$ and $b_S(\cdot) \geq 0$, each term on the right-hand side is non-negative; hence $S(t) \geq 0$ for all $t \geq 0$.

From the second equation of 1 Similarly,

$$\dot{V} = \theta\Lambda + (1-\chi)\rho Q - (\lambda_r + \mu)V.$$

Set $a_V(t) = \lambda_r(t) + \mu \geq 0$ and $b_V(t) = \theta\Lambda + (1-\chi)\rho Q(t) \geq 0$. Integrating factor yields

$$V(t) = V(0)e^{-\int_0^t a_V(s)\,ds} + \int_0^t e^{-\int_s^t a_V(u)\,du} b_V(s)\,ds \geq 0.$$

From the Third equation of 1

$$\dot{V}_E = \lambda_r V - (\pi + \mu)V_E.$$

With $a_{V_E}(t) = \pi + \mu \geq 0$ and $b_{V_E}(t) = \lambda_r(t)V(t) \geq 0$, we obtain

$$V_E(t) = V_E(0)e^{-(\pi+\mu)t} + \int_0^t e^{-(\pi+\mu)(t-s)} \lambda_r(s)V(s)\,ds \geq 0.$$

From the Fourth equation of 1

$$\dot{E} = \lambda_c S - (\alpha_1 + \alpha_2 + \alpha_3 + \mu)E.$$

Set $a_E = \alpha_1 + \alpha_2 + \alpha_3 + \mu \geq 0$ and $b_E(t) = \lambda_c(t)S(t) \geq 0$. Thus

$$E(t) = E(0)e^{-a_E t} + \int_0^t e^{-a_E(t-s)} \lambda_c(s)S(s)\,ds \geq 0.$$

From the Fifth equation of 1.

$$\dot{Q} = \alpha_1 E + \pi V_E - (\rho + \mu)Q.$$

With $a_Q = \rho + \mu \geq 0$ and $b_Q(t) = \alpha_1 E(t) + \pi V_E(t) \geq 0$, we have

$$Q(t) = Q(0)e^{-a_Q t} + \int_0^t e^{-a_Q(t-s)}\big(\alpha_1 E(s) + \pi V_E(s)\big)\,ds \geq 0.$$

From the sixth equation of 1

$$\dot{A} = \alpha_3 E - (m + \gamma_1 + \mu)A.$$

Let $a_A = m + \gamma_1 + \mu \geq 0$ and $b_A(t) = \alpha_3 E(t) \geq 0$. Then

$$A(t) = A(0)e^{-a_A t} + \int_0^t e^{-a_A(t-s)} \alpha_3 E(s)\,ds \geq 0.$$

From the Seventh equation of 1

$$\dot{I} = \alpha_2 E + \chi\rho Q + mA - (\gamma_2 + \psi + \mu + \delta)I.$$

Take $a_I = \gamma_2 + \psi + \mu + \delta \geq 0$ and $b_I(t) = \alpha_2 E(t) + \chi\rho Q(t) + mA(t) \geq 0$. Hence

$$I(t) = I(0)e^{-\int_0^t a_I\, ds} + \int_0^t e^{-\int_s^t a_I\, du}\, b_I(s)\, ds \geq 0.$$

From the eighth equation of 1.

$$\dot{H} = \psi I - (\gamma_3 + \mu + \delta)H.$$

With $a_H = \gamma_3 + \mu + \delta \geq 0$ and $b_H(t) = \psi I(t) \geq 0$, we obtain

$$H(t) = H(0)e^{-a_H t} + \int_0^t e^{-a_H(t-s)}\, \psi I(s)\, ds \geq 0.$$

From the last equation of 1.

$$\dot{R} = \gamma_1 A + \gamma_2 I + \gamma_3 H - (\phi + \mu)R.$$

Let $a_R = \phi + \mu \geq 0$ and $b_R(t) = \gamma_1 A(t) + \gamma_2 I(t) + \gamma_3 H(t) \geq 0$. Then

$$R(t) = R(0)e^{-a_R t} + \int_0^t e^{-a_R(t-s)}\big(\gamma_1 A(s) + \gamma_2 I(s) + \gamma_3 H(s)\big)\, ds \geq 0.$$

Because each compartment admits an integral representation of the form

$$X(t) = X(0)e^{-\int_0^t a_X(s)\, ds} + \int_0^t e^{-\int_s^t a_X(u)\, du}\, b_X(s)\, ds,$$

with $a_X(\cdot) \geq 0$ and $b_X(\cdot) \geq 0$, and since all initial data are non-negative, it follows that every term on the right-hand side is non-negative. Therefore each compartment satisfies $X(t) \geq 0$ for all $t \geq 0$.

Hence the solution of system 1 with non-negative initial data remains non-negative for all $t \geq 0$.

3.2 Invariant region

Here we show that the COVID–19 model 1 is epidemiologically and mathematically well-posed by proving that its solutions are positive, unique and bounded in a feasible region $\mathcal{D}$.

Theorem 3.2. *Let*

$$\mathcal{D} = \Big\{(S, V, E, V_E, Q, A, I, H, R) \in \mathbb{R}^9_+ :\ S + V + E + V_E + Q + A + I + H + R \leq \frac{\Lambda}{\mu}\Big\}.$$

Then $\mathcal{D}$ is positively invariant for system 1. In particular, for any initial condition

$$(S(0), V(0), E(0), V_E(0), Q(0), A(0), I(0), H(0), R(0)) \in \mathbb{R}^9_+,$$

the solution exists, is unique, non-negative for all $t \geq 0$, and satisfies

$$S(t) + V(t) + E(t) + V_E(t) + Q(t) + A(t) + I(t) + H(t) + R(t) \leq \frac{\Lambda}{\mu} \quad \textit{for all } t \geq 0.$$

Proof. Let

$$N(t) = S(t) + V(t) + E(t) + V_E(t) + Q(t) + A(t) + I(t) + H(t) + R(t)$$

denote the total human population in the model. Summing the right-hand sides of the equations of system 1 yields the equation for $N(t)$. Using the model structure (births/recruitment Λ, natural death μ applied to all compartments, and disease-induced deaths δ in I and H) we obtain

$$\frac{dN}{dt} = \Lambda - \mu N(t) - \delta\big(I(t) + H(t)\big). \tag{2}$$

Since $I(t), H(t) \geq 0$ for all $t \geq 0$ (by the non-negativity result established earlier), the last term on the right-hand side of (2) is non-negative. Hence we have the differential inequality

$$\frac{dN}{dt} \leq \Lambda - \mu N(t).$$

Consider the linear comparison scalar equation

$$\frac{d\widetilde{N}}{dt} = \Lambda - \mu\widetilde{N}, \qquad \widetilde{N}(0) = N(0).$$

This linear ODE has the explicit solution

$$\widetilde{N}(t) = N(0)e^{-\mu t} + \frac{\Lambda}{\mu}\big(1 - e^{-\mu t}\big).$$

By the comparison principle (or Grönwall inequality), from $\dot{N} \leq \Lambda - \mu N$ and $N(0) = \widetilde{N}(0)$ it follows that

$$N(t) \leq \widetilde{N}(t) \qquad \text{for all } t \geq 0.$$

Taking the limit $t \to \infty$ in the expression for $\widetilde{N}(t)$ gives the upper bound

$$\limsup_{t\to\infty} N(t) \leq \frac{\Lambda}{\mu},$$

and in fact for every $t \geq 0$,

$$N(t) \leq N(0)e^{-\mu t} + \frac{\Lambda}{\mu}\big(1 - e^{-\mu t}\big) \leq \frac{\Lambda}{\mu}.$$

Thus any solution that starts with $N(0) \leq \Lambda/\mu$ satisfies $N(t) \leq \Lambda/\mu$ for all $t \geq 0$. Equivalently, the set

$$\mathcal{D} = \left\{(S, \ldots, R) \in \mathbb{R}^9_+ : \ N \leq \frac{\Lambda}{\mu}\right\}$$

is forward invariant under the flow of system 1.

Positivity of each compartment (i.e., non-negativity for all $t \geq 0$) was proved in the previous section (integrating factor argument); therefore solutions starting in $\mathcal{D}$ remain in $\mathcal{D}$ for all time.

Finally, standard existence and uniqueness results for autonomous ODE systems apply because the right-hand side of system 1 is continuously differentiable (hence locally Lipschitz) on $\mathbb{R}^9$. Consequently, for any initial data in $\mathbb{R}^9_+$ there exists a unique solution defined on a maximal interval of existence; the above bounds show this solution is global in time and remains in $\mathcal{D}$. This completes the proof. □

3.3 Disease-Free Equilibrium (DFE)

At the DFE, there is no disease:

$$E = Q = V_E = I = A = H = 0.$$

The system reduces to:

$$\frac{dS}{dt} = (1-\theta)\Lambda + \phi R - \mu S = 0, \quad \frac{dV}{dt} = \theta\Lambda - \mu V = 0, \quad \frac{dR}{dt} = -(\phi+\mu)R = 0.$$

Solving gives:

$$S^0 = \frac{(1-\theta)\Lambda}{\mu}, \quad V^0 = \frac{\theta\Lambda}{\mu}, \quad R^0 = 0.$$

Thus, the DFE is:

$$\epsilon_0 = (S^0, V^0, V_E^0, E^0, Q^0, I^0, A^0, H^0, R^0) = \left(\frac{(1-\theta)\Lambda}{\mu}, \frac{\theta\Lambda}{\mu}, 0, 0, 0, 0, 0, 0, 0\right).$$

3.4 Basic reproduction number R_0 of the model

The basic reproduction number is the average number of secondary infections caused by a typical infections individual in a completely susceptible population. To obtain this,we adapt the next generation matrix method described by Vanden and Watmough (2002).
The infected compartments are $X = (E, V_E, Q, I, A, H)^T$.
Then our model can be written as

$$\frac{d\mathcal{X}}{dt} = f(x) - v(x) \tag{3}$$

where $f(x)$ is the ratio of appearance of new infection into the disease compartments while the $v(x)$ is the rate of transfer of individuals in and out of the disease compartments, it is defined as

$$v(x) = v^-(x) - v^+(x)$$

$$f(x) = \begin{pmatrix} \lambda_c S \\ \lambda_r V \\ 0 \\ 0 \\ 0 \\ 0 \end{pmatrix}, \quad v(x) = \begin{pmatrix} (\alpha_1+\alpha_2+\alpha_3+\mu)\,E \\ (\pi+\mu)V_E \\ -\alpha_1 E - \pi V_E + (\rho+\mu)Q \\ -\alpha_2 E - \chi\rho Q - mA + (\gamma_2+\psi+\mu+\delta)I \\ -\alpha_3 E - (m+\gamma_1+\mu)A \\ -\psi I - (\gamma_3+\mu+\delta)H \end{pmatrix}$$

$$F = \begin{pmatrix} 0 & 0 & 0 & \frac{\beta_c S^0}{N^0} & \frac{\beta_c \eta_A S^0}{N^0} & \frac{\beta_c \eta_H S^0}{N^0} \\ 0 & 0 & 0 & \frac{\beta_r(1-\epsilon)V^0}{N^0} & \frac{\beta_r(1-\epsilon)\eta_A V^0}{N^0} & \frac{\beta_r(1-\epsilon)\eta_H V^0}{N^0} \\ 0 & 0 & 0 & 0 & 0 & 0 \\ 0 & 0 & 0 & 0 & 0 & 0 \\ 0 & 0 & 0 & 0 & 0 & 0 \\ 0 & 0 & 0 & 0 & 0 & 0 \end{pmatrix}, \quad V = \begin{pmatrix} k_1 & 0 & 0 & 0 & 0 & 0 \\ 0 & k_2 & 0 & 0 & 0 & 0 \\ -\alpha_1 & -\pi & k_3 & 0 & 0 & 0 \\ -\alpha_2 & 0 & -\chi\rho & k_4 & -m & 0 \\ -\alpha_3 & 0 & 0 & 0 & k_5 & 0 \\ 0 & 0 & 0 & -\psi & 0 & k_6 \end{pmatrix},$$

where:

$k_1 = \alpha_1+\alpha_2+\alpha_3+\mu, \quad k_2 = \pi+\mu, \quad k_3 = \rho+\mu, \quad k_4 = \gamma_2+\psi+\mu+\delta, \quad k_5 = m+\gamma_1+\mu, \quad k_6 = \gamma_3+\mu+\delta.$

The next generation matrix is $K = FV^{-1}$.
The basic reproduction number $R_0 = \rho(K)$ for the model is given by:

$$R_0 = R_c + R_v,$$

where

$$R_c = \beta_c(1-\theta)\left[\frac{\alpha_2}{k_1k_4} + \frac{\alpha_3\eta_A}{k_1k_5} + \frac{\alpha_1\chi\rho}{k_1k_3k_4} + \frac{\alpha_2\psi\eta_H}{k_1k_4k_6} + \frac{\alpha_1\chi\rho\psi\eta_H}{k_1k_3k_4k_6}\right],$$

$$R_v = \beta_r(1-\epsilon)\theta\left[\frac{\pi\chi\rho}{k_2k_3k_4} + \frac{\pi\chi\rho\psi\eta_H}{k_2k_3k_4k_6}\right],$$

Note that R_c is the contribution from the unvaccinated population and R_v is the contribution from the vaccinated population.

$$R_0 = \beta_c(1-\theta)\left[\frac{\alpha_2}{k_1k_4} + \frac{\alpha_3\eta_A}{k_1k_5} + \frac{\alpha_1\chi\rho}{k_1k_3k_4} + \frac{\alpha_2\psi\eta_H}{k_1k_4k_6} + \frac{\alpha_1\chi\rho\psi\eta_H}{k_1k_3k_4k_6}\right] + \beta_r(1-\epsilon)\theta\left[\frac{\pi\chi\rho}{k_2k_3k_4} + \frac{\pi\chi\rho\psi\eta_H}{k_2k_3k_4k_6}\right],$$

where

$$\begin{aligned}
k_1 &= \alpha_1 + \alpha_2 + \alpha_3 + \mu,\\
k_2 &= \pi + \mu,\\
k_3 &= \rho + \mu,\\
k_4 &= \gamma_2 + \psi + \mu + \delta,\\
k_5 &= m + \gamma_1 + \mu,\\
k_6 &= \gamma_3 + \mu + \delta.
\end{aligned}$$

3.5 Local stability of the disease - free equilibrium

Theorem: The disease-free steady state, ε_0 is locally asymptomatically stable if $R_o < 1$ and unstable if $R_o > 1$.

The Jacobian matrix of the COVID-19 model at the Disease-Free Equilibrium is:

$$J = \begin{bmatrix}
-\mu & 0 & 0 & 0 & 0 & -S_0\frac{\beta_c\eta_A}{N_0} & -S_0\frac{\beta_c}{N_0} & -S_0\frac{\beta_c\eta_H}{N_0} & \phi\\
0 & -\mu & 0 & 0 & (1-\chi)\rho & -V_0\frac{\beta_r(1-\varepsilon)\eta_A}{N_0} & -V_0\frac{\beta_r(1-\varepsilon)}{N_0} & -V_0\frac{\beta_r(1-\varepsilon)\eta_H}{N_0} & 0\\
0 & 0 & -K_1 & 0 & 0 & V_0\frac{\beta_r(1-\varepsilon)\eta_A}{N_0} & V_0\frac{\beta_r(1-\varepsilon)}{N_0} & V_0\frac{\beta_r(1-\varepsilon)\eta_H}{N_0} & 0\\
0 & 0 & 0 & -K2 & 0 & S_0\frac{\beta_c\eta_A}{N_0} & S_0\frac{\beta_c}{N_0} & S_0\frac{\beta_c\eta_H}{N_0} & 0\\
0 & 0 & \pi & \alpha_1 & -K_3 & 0 & 0 & 0 & 0\\
0 & 0 & 0 & \alpha_3 & 0 & -K_4 & 0 & 0 & 0\\
0 & 0 & 0 & \alpha_2 & \chi\rho & m & -K_5 & 0 & 0\\
0 & 0 & 0 & 0 & 0 & 0 & \psi & -K_6 & 0\\
0 & 0 & 0 & 0 & 0 & \gamma_1 & \gamma_2 & \gamma_3 & -K_7
\end{bmatrix}$$

where

$$\begin{aligned}
K_1 &= \pi + \mu,\\
K_2 &= \alpha_1 + \alpha_2 + \alpha_3 + \mu,\\
K_3 &= \rho + \mu,\\
K_4 &= \gamma_2 + \psi + \mu + \delta,\\
K_5 &= m + \gamma_1 + \mu,\\
K_6 &= \gamma_3 + \mu + \delta\\
K_7 &= \phi + \mu.
\end{aligned}$$

The Jacobian matrix at the DFE is block-decomposed as:

$$J = \begin{pmatrix} J_{11} & J_{12} \\ 0 & J_{22} \end{pmatrix},$$

where J_{11} corresponds to the non-infected compartments (S, V, R) and J_{22} corresponds to the infected compartments (V_E, E, Q, I, A, H).

Eigenvalues from J_{11}

$$J_{11} = \begin{pmatrix} -\mu & 0 & \phi \\ 0 & -\mu & 0 \\ 0 & 0 & -K_7 \end{pmatrix}.$$

This is lower triangular, with eigenvalues:

$$\lambda_1 = -\mu, \quad \lambda_2 = -\mu, \quad \lambda_3 = -K_7.$$

All are negative.

Eigenvalues from J_{22}

$$J_{22} = \begin{pmatrix} -k_1 & 0 & 0 & \frac{\beta_r(1-\epsilon)V^0}{N^0} & \frac{\beta_r(1-\epsilon)\eta_A V^0}{N^0} & \frac{\beta_r(1-\epsilon)\eta_H V^0}{N^0} \\ 0 & -k_2 & 0 & \frac{\beta_c S^0}{N^0} & \frac{\beta_c \eta_A S^0}{N^0} & \frac{\beta_c \eta_H S^0}{N^0} \\ \pi & \alpha_1 & -k_3 & 0 & 0 & 0 \\ 0 & \alpha_2 & \chi\rho & -k_4 & m & 0 \\ 0 & \alpha_3 & 0 & 0 & -k_5 & 0 \\ 0 & 0 & 0 & \psi & 0 & -k_6 \end{pmatrix}.$$

From the next-generation matrix method, the eigenvalues of J_{22} have negative real parts if and only if $R_0 < 1$.

Conclusion

Since all eigenvalues from J_{11} are negative and those from J_{22} have negative real parts when $R_0 < 1$, the entire Jacobian J has eigenvalues with negative real parts if $R_0 < 1$. Therefore, the DFE is locally asymptotically stable if: $\rho(FV^{-1}) < 1$.

3.6 Global Stability Analysis of the Disease Free Equilibrium

Theorem 3.3. *The disease-free equilibrium of model* (2.1) *is globally asymptotically stable in D if* $R_0 \leq 1$.

Consider the Lyapunov function:

$$L = C_1E + C_2V_E + C_3Q + C_4I + C_5A + C_6H,$$

where $C_1, C_2, C_3, C_4, C_5, C_6 > 0$ are constants to be determined.

The time derivative is:

$$\begin{aligned} \frac{dL}{dt} &= C_1(\lambda_c S - k_1 E) + C_2(\lambda_r V - k_2 V_E) + C_3(\alpha_1 E + \pi V_E - k_3 Q) \\ &\quad + C_4(\alpha_2 E + \chi\rho Q + mA - k_4 I) + C_5(\alpha_3 E - k_5 A) + C_6(\psi I - k_6 H). \end{aligned}$$

Group terms:

$$\begin{aligned}\frac{dL}{dt} = &[C_1\lambda_c S + C_2\lambda_r V] \\ &+ E[-C_1k_1 + C_3\alpha_1 + C_4\alpha_2 + C_5\alpha_3] \\ &+ V_E[-C_2k_2 + C_3\pi] \\ &+ Q[-C_3k_3 + C_4\chi\rho] \\ &+ I[-C_4k_4 + C_6\psi] \\ &+ A[C_4m - C_5k_5] \\ &+ H[-C_6k_6].\end{aligned}$$

Choose constants to eliminate positive terms:

$$\begin{aligned}C_3\alpha_1 + C_4\alpha_2 + C_5\alpha_3 &= C_1k_1, \\ C_3\pi &= C_2k_2, \\ C_4\chi\rho &= C_3k_3, \\ C_6\psi &= C_4k_4, \\ C_4m &= C_5k_5.\end{aligned}$$

Let $C_4 = 1$, then:

$$\begin{aligned}C_6 &= \frac{k_4}{\psi}, \\ C_5 &= \frac{m}{k_5}, \\ C_3 &= \frac{\chi\rho}{k_3}, \\ C_2 &= \frac{\chi\rho\pi}{k_2k_3}, \\ C_1 &= \frac{\frac{\chi\rho}{k_3}\alpha_1 + \alpha_2 + \frac{m}{k_5}\alpha_3}{k_1}.\end{aligned}$$

Now:

$$C_1\lambda_c S + C_2\lambda_r V = \frac{I + \eta_A A + \eta_H H}{N}\left(C_1\beta_c S + C_2\beta_r(1-\epsilon)V\right).$$

Since $S \leq S^0$, $V \leq V^0$, $N \geq N^0$:

$$C_1\lambda_c S + C_2\lambda_r V \leq \frac{I + \eta_A A + \eta_H H}{N^0}\left(C_1\beta_c S^0 + C_2\beta_r(1-\epsilon)V^0\right).$$

With the chosen constants, $C_1\beta_c S^0 + C_2\beta_r(1-\epsilon)V^0 = R_0$. Thus:

$$\frac{dL}{dt} \leq (R_0 - 1)(I + \eta_A A + \eta_H H) - \text{positive terms}.$$

If $R_0 < 1$, then $\frac{dL}{dt} \leq 0$, and $\frac{dL}{dt} = 0$ only at the DFE. Therefore, the DFE is globally asymptotically stable when $R_0 < 1$.

3.7 Global stability analysis of the endemic equilibrium

To establish global stability of the endemic equilibrium $E^* = (S^*, V^*, V_E^*, E^*, Q^*, I^*, A^*, H^*, R^*)$, we consider the complete Lyapunov function considering all compartments:

$$\begin{aligned}\mathcal{L} =& C_1\left(S - S^* - S^*\ln\frac{S}{S^*}\right) + C_2\left(V - V^* - V^*\ln\frac{V}{V^*}\right) + C_3\left(E - E^* - E^*\ln\frac{E}{E^*}\right)\\ &+ C_4\left(V_E - V_E^* - V_E^*\ln\frac{V_E}{V_E^*}\right) + C_5\left(Q - Q^* - Q^*\ln\frac{Q}{Q^*}\right) + C_6\left(I - I^* - I^*\ln\frac{I}{I^*}\right)\\ &+ C_7\left(A - A^* - A^*\ln\frac{A}{A^*}\right) + C_8\left(H - H^* - H^*\ln\frac{H}{H^*}\right) + C_9\left(R - R^* - R^*\ln\frac{R}{R^*}\right),\end{aligned} \tag{4}$$

$$\begin{aligned}\mathcal{L} =& C_1\left(1 - \frac{S^*}{S}\right)\dot{S} + C_2\left(1 - \frac{V^*}{V}\right)\dot{V} + C_3\left(1 - \frac{E^*}{E}\right)\dot{E} + C_4\left(1 - \frac{V_E^*}{V_E}\right)\dot{V_E} + C_5\left(1 - \frac{Q^*}{Q}\right)\dot{Q}\\ &+ C_6\left(1 - \frac{A^*}{A}\right)\dot{A} + C_7\left(1 - \frac{I^*}{I}\right)\dot{I} + C_8\left(1 - \frac{H^*}{H}\right)\dot{H} + C_9\left(1 - \frac{R^*}{R}\right)\dot{R}\end{aligned}$$

where $C_1, C_2, C_3, C_4, C_5, C_6, C_7, C_8, C_9 > 0$ are constants to be determined. Then

$$\begin{aligned}\mathcal{L} =& C_1\left(1 - \frac{S^*}{S}\right)\left(\Lambda - \theta\Lambda + \phi R - \lambda_c S - \mu S\right) + C_2\left(1 - \frac{V^*}{V}\right)\left(\theta\Lambda + \rho Q - \chi\rho Q - \lambda_r V - \mu V\right)\\ &+ C_3\left(1 - \frac{E^*}{E}\right)\left(\lambda_c S - K_1 E\right) + C_4\left(1 - \frac{V_E^*}{V_E}\right)\left(\lambda_r V - K_2 V_E\right)\\ &+ C_5\left(1 - \frac{Q^*}{Q}\right)\left(\alpha_1 E + \pi V_E - K_3 Q\right) + C_6\left(1 - \frac{A^*}{A}\right)\left(\alpha_3 E - K_5 A\right)\\ &+ C_7\left(1 - \frac{I^*}{I}\right)\left(\alpha_2 E + \chi\rho Q + mA - K_4 I\right) + C_8\left(1 - \frac{H^*}{H}\right)\left(\psi I - K_6 H\right)\\ &+ C_9\left(1 - \frac{R^*}{R}\right)\left(\gamma_1 A + \gamma_2 I + \gamma_3 H - K_7 R\right).\end{aligned}$$

At equilibrium E^*:

$$\begin{aligned}(1-\theta)\Lambda + \phi R^* &= \lambda_c^* S^* + \mu S^*,\\ \theta\Lambda + (1-\chi)\rho Q^* &= \lambda_r^* V^* + \mu V^*,\\ \lambda_r^* V^* &= (\pi + \mu)V_E^*,\\ \lambda_c^* S^* &= k_1 E^*,\\ \alpha_1 E^* + \pi V_E^* &= k_3 Q^*,\\ \alpha_2 E^* + \chi\rho Q^* + mA^* &= k_4 I^*,\\ \alpha_3 E^* &= k_5 A^*,\\ \psi I^* &= k_6 H^*,\\ \gamma_1 A^* + \gamma_2 I^* + \gamma_3 H^* &= (\phi + \mu)R^*.\end{aligned}$$

After computation of the constants, we set $C_1 = 1$ and solving the system to eliminate cross terms

yields:

$$
\begin{aligned}
C_1 &= 1,\\
C_2 &= 1,\\
C_3 &= \frac{k_1 E^*}{\lambda_c^* S^*},\\
C_4 &= \frac{(\pi+\mu)V_E^*}{\lambda_r^* V^*},\\
C_5 &= \frac{k_3 Q^*}{\alpha_1 E^* + \pi V_E^*},\\
C_6 &= 1,\\
C_7 &= \frac{k_5 A^*}{\alpha_3 E^*},\\
C_8 &= \frac{k_6 H^*}{\psi I^*},\\
C_9 &= \frac{(\phi+\mu)R^*}{\gamma_1 A^* + \gamma_2 I^* + \gamma_3 H^*}.
\end{aligned}
$$

Substituting $C_1, \ldots, C_9$ in equation (6), we have:

$$
\begin{aligned}
\mathcal{L} = {} & 1\left[\left(1-\frac{S^*}{S}\right)\left(\Lambda-\theta\Lambda+\phi R-\lambda_c S-\mu S\right)\right] + 1\left[\left(1-\frac{V^*}{V}\right)\left(\theta\Lambda+\rho Q-\chi\rho Q-\lambda_r V-\mu V\right)\right]\\
& + \frac{k_1 E^*}{\lambda_c^* S^*}\left[\left(1-\frac{E^*}{E}\right)\left(\lambda_c S-K_1 E\right)\right] + \frac{(\pi+\mu)V_E^*}{\lambda_r^* V^*}\left[\left(1-\frac{V_E^*}{V_E}\right)\left(\lambda_r V-K_2 V_E\right)\right]\\
& + \frac{k_3 Q^*}{\alpha_1 E^* + \pi V_E^*}\left[\left(1-\frac{Q^*}{Q}\right)\left(\alpha_1 E+\pi V_E-K_3 Q\right)\right] + 1\left[\left(1-\frac{A^*}{A}\right)\left(\alpha_3 E-K_5 A\right)\right]\\
& + \frac{k_5 A^*}{\alpha_3 E^*}\left[\left(1-\frac{I^*}{I}\right)\left(\alpha_2 E+\chi\rho Q+mA-K_4 I\right)\right] + \frac{k_6 H^*}{\psi I^*}\left[\left(1-\frac{H^*}{H}\right)\left(\psi I-K_6 H\right)\right]\\
& + \frac{(\phi+\mu)R^*}{\gamma_1 A^* + \gamma_2 I^* + \gamma_3 H^*}\left[\left(1-\frac{R^*}{R}\right)\left(\gamma_1 A+\gamma_2 I+\gamma_3 H-K_7 R\right)\right]
\end{aligned}
$$

$$
\begin{aligned}
\mathcal{L} = {} & 1\left[\Lambda-\theta\Lambda+\phi R-\lambda_c S-\mu S-\frac{\Lambda S^*}{S}+\frac{\theta R S^*}{S}-\frac{\phi R S^*}{S}+\lambda_c S^*+\mu S^*\right]\\
& + 1\left[\theta\Lambda+\rho Q-\rho\chi Q-\lambda_r V-\mu V-\frac{\theta\Lambda V^*}{V}-\frac{\rho Q V^*}{V}+\frac{\rho\chi Q V^*}{V}+\lambda_r V^*+\mu V^*\right]\\
& + \frac{k_1 E^*}{\lambda_c^* S^*}\left[\lambda_c S-K_1 E-\frac{\lambda_c S E^*}{E}+K_1 E^*\right]\\
& + \frac{(\pi+\mu)V_E^*}{\lambda_r^* V^*}\left[\lambda_r V-\pi V_E-\mu V_E-\frac{\lambda_r V V_E^*}{V_E}+\pi V_E^*+\mu V_E^*\right]\\
& + \frac{k_3 Q^*}{\alpha_1 E^* + \pi V_E^*}\left[\alpha_1 E+\pi V_E-K_3 Q-\frac{\alpha_1 E Q^*}{Q}-\frac{\pi V_E Q^*}{Q}+K_3 Q^*\right]\\
& + 1\left[\alpha_3 E-K_5 A-\frac{\alpha_3 E A^*}{A}+K_5 A^*\right]\\
& + \frac{k_5 A^*}{\alpha_3 E^*}\left[\alpha_2 E+\chi\rho Q+mA-K_4 I-\frac{\alpha_2 E I^*}{I}-\frac{\chi\rho Q I^*}{I}-\frac{mA I^*}{I}+K_4 I^*\right]\\
& + \frac{k_6 H^*}{\psi I^*}\left[\psi I-K_6 H-\frac{\psi I H^*}{H}+K_6 H^*\right]\\
& + \frac{(\phi+\mu)R^*}{\gamma_1 A^* + \gamma_2 I^* + \gamma_3 H^*}\left[\gamma_1 A+\gamma_2 I+\gamma_3 H-K_7 R-\frac{\gamma_1 A R^*}{R}-\frac{\gamma_2 I R^*}{R}-\frac{\gamma_3 H R^*}{R}+K_7 R^*\right]
\end{aligned}
$$

$$
\begin{aligned}
\mathcal{L} = &\left[\Lambda + \phi R - \frac{\theta\Lambda V^*}{V} - \frac{\rho Q V^*}{V} + \frac{\rho\chi Q V^*}{V} + \rho Q - \rho\chi Q - \lambda_r V + \lambda_r V^* + \mu V^* - \mu V\right] \\
&\left[\lambda_c S^* - \frac{\Lambda S^*}{S} + \frac{\theta R S^*}{S} - \frac{\phi R S^*}{S} - \lambda_c S - \mu S + \mu S^*\right] \\
&+ \frac{k_1 E^*}{\lambda_c^* S^*}\left[\lambda_c S - K_1 E - \frac{\lambda_c S E^*}{E} + K_1 E^*\right] \\
&+ \frac{(\pi+\mu)V_E^*}{\lambda_r^* V^*}\left[\lambda_r V - \pi V_E - \mu V_E - \frac{\lambda_r V V_E^*}{V_E} + \pi V_E^* + \mu V_E^*\right] \\
&+ \frac{k_3 Q^*}{\alpha_1 E^* + \pi V_E^*}\left[\alpha_1 E + \pi V_E - K_3 Q - \frac{\alpha_1 E Q^*}{Q} - \frac{\pi V_E Q^*}{Q} + K_3 Q^*\right] \\
&+ 1\left[\alpha_3 E - K_5 A - \frac{\alpha_3 E A^*}{A} + K_5 A^*\right] \\
&+ \frac{k_5 A^*}{\alpha_3 E^*}\left[\alpha_2 E + \chi\rho Q + mA - K_4 I - \frac{\alpha_2 E I^*}{I} - \frac{\chi\rho Q I^*}{I} - \frac{mAI^*}{I} + K_4 I^*\right] \\
&+ \frac{k_6 H^*}{\psi I^*}\left[\psi I - K_6 H - \frac{\psi I H^*}{H} + K_6 H^*\right] \\
&+ \frac{(\phi+\mu)R^*}{\gamma_1 A^* + \gamma_2 I^* + \gamma_3 H^*}\left[\gamma_1 A + \gamma_2 I + \gamma_3 H - K_7 R - \frac{\gamma_1 A R^*}{R} - \frac{\gamma_2 I R^*}{R} - \frac{\gamma_3 H R^*}{R} + K_7 R^*\right]
\end{aligned}
$$

As arithmetic mean is greater that geometric mean, the following inequalities from (9) hold:

$$
\begin{aligned}
&\left(\Lambda + \phi R - \frac{\theta\Lambda V^*}{V} - \frac{\rho Q V^*}{V} + \frac{\rho\chi Q V^*}{V} + \rho Q - \rho\chi Q - \lambda_r V + \lambda_r V^* + \mu V^* - \mu V\right) \leq 0, \\
&\left(\lambda_c S^* - \frac{\Lambda S^*}{S} + \frac{\theta R S^*}{S} - \frac{\phi R S^*}{S} - \lambda_c S - \mu S + \mu S^*\right) \leq 0, \\
&\left(\lambda_c S - K_1 E - \frac{\lambda_c S E^*}{E} + K_1 E^*\right) \leq 0, \\
&\left(\lambda_r V - \pi V_E - \mu V_E - \frac{\lambda_r V V_E^*}{V_E} + \pi V_E^* + \mu V_E^*\right) \leq 0, \\
&\left(\alpha_1 E + \pi V_E - K_3 Q - \frac{\alpha_1 E Q^*}{Q} - \frac{\pi V_E Q^*}{Q} + K_3 Q^*\right) \leq 0, \\
&\left(\alpha_3 E - K_5 A - \frac{\alpha_3 E A^*}{A} + K_5 A^*\right) \leq 0, \\
&\left(\alpha_2 E + \chi\rho Q + mA - K_4 I - \frac{\alpha_2 E I^*}{I} - \frac{\chi\rho Q I^*}{I} - \frac{mAI^*}{I} + K_4 I^*\right) \leq 0, \\
&\left(\psi I - K_6 H - \frac{\psi I H^*}{H} + K_6 H^*\right) \leq 0, \\
&\left(\gamma_1 A + \gamma_2 I + \gamma_3 H - K_7 R - \frac{\gamma_1 A R^*}{R} - \frac{\gamma_2 I R^*}{R} - \frac{\gamma_3 H R^*}{R} + K_7 R^*\right) \leq 0
\end{aligned}
$$

Hence, $\dot{\mathcal{L}} \leq 0$ for $\bar{R}_0 > 1$. Therefore, $\mathcal{L}$ is a Lyapunov function in D and it concluded that the GAS of EEP is globally asymptotically stable for $\bar{R}_0 > 1$.

The global stability of the endemic equilibrium, demonstrated through an appropriate Lyapunov function, indicates that when the basic reproduction number $R_0 > 1$, COVID-19 will persist within the population at a stable endemic level over time, regardless of initial conditions. This conclusion remains valid even considering breakthrough infections resulting from vaccination and reinfections, both of

which contribute to ongoing transmission dynamics in the post-vaccination phase. Although COVID-19 is no longer classified as a global public health emergency, this mathematical observation suggests the likelihood of the virus continuing to circulate at low to moderate levels within communities. The global stability of the endemic equilibrium highlights that, unless sufficient immunity or control measures can lower R_0 below one, the virus is unlikely to be eradicated and will instead establish a consistent and enduring presence. This scenario underscores the importance of ongoing surveillance, periodic booster vaccinations, and targeted interventions to effectively manage COVID-19 as an endemic condition.

4 Sensitivity analysis of the basic reproduction number

Sensitivity analysis is an important aspect of epidemiological modeling as it assesses how changes in model parameters influence key outcomes. Specifically, in compartmental infectious disease models, it offers a structured approach to identifying the parameters that most significantly affect the basic reproduction number R_0, a critical metric for determining whether an infection can spread and maintain itself in a population. By ranking the significance of these parameters, sensitivity analysis reveals which biological or intervention-related processes are the primary drivers of transmission, thus informing the prioritization of control measures and policy actions.

In this study, we conducted a comprehensive sensitivity analysis of our co-infection model to assess the impact of variations in selected parameters on R_O. We focused on parameters that have direct implications for policy, including the human-to-human transmission rate β_c, the vaccination uptake rate θ, the vaccinated transmission rate β_r, and the rates linked to disease progression, treatment, and recovery. Analyzing these parameters aids in understanding the processes of transmission, vaccination, recovery, or quarantine that most significantly affect the potential for disease spread.

The normalized sensitivity index of R_0 in relation to each parameter p was calculated using the standard formula.

$$S_p^{\mathcal{R}_0} = \frac{\partial \mathcal{R}_0}{\partial p}\frac{p}{\mathcal{R}_0}$$

To determine the value of (R_0), we employed the model parameters outlined and referenced in Table 5 below.

$$R_0 = \beta_c(1-\theta)\left[\frac{\alpha_2}{k_1k_4} + \frac{\alpha_3\eta_A}{k_1k_5} + \frac{\alpha_1\chi\rho}{k_1k_3k_4} + \frac{\alpha_2\psi\eta_H}{k_1k_4k_6} + \frac{\alpha_1\chi\rho\psi\eta_H}{k_1k_3k_4k_6}\right] + \beta_r(1-\epsilon)\theta\left[\frac{\pi\chi\rho}{k_2k_3k_4} + \frac{\pi\chi\rho\psi\eta_H}{k_2k_3k_4k_6}\right]$$

Let $R_0 = T_1 + T_2$, where:

$$T_1 = \beta_c(1-\theta)A$$
$$T_2 = \beta_r(1-\epsilon)\theta B$$

with:

$$A = \frac{\alpha_2}{k_1k_4} + \frac{\alpha_3\eta_A}{k_1k_5} + \frac{\alpha_1\chi\rho}{k_1k_3k_4} + \frac{\alpha_2\psi\eta_H}{k_1k_4k_6} + \frac{\alpha_1\chi\rho\psi\eta_H}{k_1k_3k_4k_6}$$
$$B = \frac{\pi\chi\rho}{k_2k_3k_4} + \frac{\pi\chi\rho\psi\eta_H}{k_2k_3k_4k_6}$$

First, compute A and B:

$$\begin{aligned} A &= \frac{0.18}{0.580040\times 0.125040} + \frac{0.25\times 0.45}{0.580040\times 0.170040} + \frac{0.15\times 0.2\times 0.2}{0.580040\times 0.200040\times 0.125040} \\ &\quad + \frac{0.18\times 0.02\times 0.10}{0.580040\times 0.125040\times 0.075040} + \frac{0.15\times 0.2\times 0.2\times 0.02\times 0.10}{0.580040\times 0.200040\times 0.125040\times 0.075040} \\ &= 2.482 + 1.141 + 0.414 + 0.066 + 0.011 = 4.114 \end{aligned}$$

$$B = \frac{0.10 \times 0.2 \times 0.2}{0.100040 \times 0.200040 \times 0.125040} + \frac{0.10 \times 0.2 \times 0.2 \times 0.02 \times 0.10}{0.100040 \times 0.200040 \times 0.125040 \times 0.075040}$$
$$= 1.599 + 0.043 = 1.642$$

Now compute R_0:

$$R_0 = 0.28 \times (1 - 0.15) \times 4.114 + 0.15 \times (1 - 0.65) \times 0.15 \times 1.642$$
$$= 0.28 \times 0.85 \times 4.114 + 0.15 \times 0.35 \times 0.15 \times 1.642$$
$$= 0.979 + 0.013 = 0.992$$

Sensitivity to β_c

$$\frac{\partial R_0}{\partial \beta_c} = (1 - \theta)A = 3.497$$

$$S_{\beta_c} = \frac{\partial R_0}{\partial \beta_c} \cdot \frac{\beta_c}{R_0} = \frac{\beta_c(1 - \theta)A}{R_0} = 0.987$$

Sensitivity to θ

$$\frac{\partial R_0}{\partial \theta} = -\beta_c A + \beta_r(1 - \epsilon)B = -1.094$$

$$S_\theta = \frac{\partial R_0}{\partial \theta} \cdot \frac{\theta}{R_0} = -0.165$$

Sensitivity to β_r

$$\frac{\partial R_0}{\partial \beta_r} = (1 - \epsilon)\theta B = 0.086$$

$$S_{\beta_r} = \frac{\partial R_0}{\partial \beta_r} \cdot \frac{\beta_r}{R_0} = 0.013$$

Sensitivity to ε

$$\frac{\partial R_0}{\partial \varepsilon} = -\beta_r \theta B = -0.037$$

$$S_\varepsilon = \frac{\partial R_0}{\partial \varepsilon} \cdot \frac{\varepsilon}{R_0} = -0.024$$

Sensitivity to α_1

$$\frac{\partial R_0}{\partial \alpha_1} = \beta_c(1 - \theta)\left[\frac{\chi\rho}{k_1 k_3 k_4} + \frac{\chi\rho\psi\eta_H}{k_1 k_3 k_4 k_6} - \frac{A}{k_1}\right] = 0.275$$

$$S_{\alpha_1} = \frac{\partial R_0}{\partial \alpha_1} \cdot \frac{\alpha_1}{R_0} = 0.042$$

Sensitivity to α_2

$$\frac{\partial R_0}{\partial \alpha_2} = \beta_c(1 - \theta)\left[\frac{1}{k_1 k_4} + \frac{\psi\eta_H}{k_1 k_4 k_6} - \frac{A}{k_1}\right] = 0.369$$

$$S_{\alpha_2} = \frac{\partial R_0}{\partial \alpha_2} \cdot \frac{\alpha_2}{R_0} = 0.067$$

Sensitivity to α_3

$$\frac{\partial R_0}{\partial \alpha_3} = \beta_c(1-\theta)\left[\frac{\eta_A}{k_1k_5} - \frac{A}{k_1}\right] = 0.493$$

$$S_{\alpha_3} = \frac{\partial R_0}{\partial \alpha_3}\cdot\frac{\alpha_3}{R_0} = 0.124$$

Sensitivity to η_A

$$\frac{\partial R_0}{\partial \eta_A} = \beta_c(1-\theta)\cdot\frac{\alpha_3}{k_1k_5} = 1.141$$

$$S_{\eta_A} = \frac{\partial R_0}{\partial \eta_A}\cdot\frac{\eta_A}{R_0} = 0.518$$

Sensitivity to η_H

$$\frac{\partial R_0}{\partial \eta_H} = \beta_c(1-\theta)\left[\frac{\alpha_2\psi}{k_1k_4k_6} + \frac{\alpha_1\chi\rho\psi}{k_1k_3k_4k_6}\right] + \beta_r(1-\epsilon)\theta\cdot\frac{\pi\chi\rho\psi}{k_2k_3k_4k_6} = 0.423$$

$$S_{\eta_H} = \frac{\partial R_0}{\partial \eta_H}\cdot\frac{\eta_H}{R_0} = 0.043$$

Sensitivity to π

$$\frac{\partial R_0}{\partial \pi} = \beta_r(1-\epsilon)\theta\left[\frac{\chi\rho}{k_2k_3k_4} + \frac{\chi\rho\psi\eta_H}{k_2k_3k_4k_6} - \frac{B}{k_2}\right] = 0.246$$

$$S_{\pi} = \frac{\partial R_0}{\partial \chi}\cdot\frac{\pi}{R_0} = 0.025$$

Sensitivity to χ

$$\frac{\partial R_0}{\partial \chi} = \frac{\beta_c(1-\theta)}{\chi}\left(A - \frac{\alpha_2}{k_1k_4} - \frac{\alpha_3\eta_A}{k_1k_5} - \frac{\alpha_2\psi\eta_H}{k_1k_4k_6}\right) + \frac{\beta_r(1-\epsilon)\theta}{\chi}B = 0.329$$

$$S_{\chi} = \frac{\partial R_0}{\partial \chi}\cdot\frac{\chi}{R_0} = 0.066$$

Sensitivity to Recovery Rates $\gamma_1, \gamma_2, \gamma_3$

For γ_1:

$$\frac{\partial R_0}{\partial \gamma_1} = -\beta_c(1-\theta)\frac{\alpha_3\eta_A}{k_1k_5^2} = -1.892$$

$$S_{\gamma_1} = \frac{\partial R_0}{\partial \gamma_1}\cdot\frac{\gamma_1}{R_0} = -0.267$$

For γ_2:

$$\frac{\partial R_0}{\partial \gamma_2} = -\beta_c(1-\theta)\frac{A}{k_4} - \beta_r(1-\epsilon)\theta\frac{B}{k_4} = -3.142$$

$$S_{\gamma_2} = \frac{\partial R_0}{\partial \gamma_2}\cdot\frac{\gamma_2}{R_0} = -0.317$$

For γ_3:

$$\frac{\partial R_0}{\partial \gamma_3} = -\beta_c(1-\theta)\left[\frac{\alpha_2\psi\eta_H}{k_1k_4k_6^2} + \frac{\alpha_1\chi\rho\psi\eta_H}{k_1k_3k_4k_6^2}\right] - \beta_r(1-\epsilon)\theta\frac{\pi\chi\rho\psi\eta_H}{k_2k_3k_4k_6^2} = -0.423$$

$$S_{\gamma_3} = \frac{\partial R_0}{\partial \gamma_3}\cdot\frac{\gamma_3}{R_0} = -0.032$$

Table 3: The Effect of the COVID-19 Parameters on $R_0 = 0.992$.

Parameters	Baseline value	$\frac{\partial R_0}{\partial p}$	Sensitivity S_p	Effect on R_0
β_c	0.28 day^{-1}	3.497	0.987	Positive
θ	0.15	-1.094	-0.165	Negative
β_r	0.15 day^{-1}	0.086	0.013	Positive
ε	0.65	-0.037	-0.024	Negative
α_2	0.18 day^{-1}	0.369	0.067	Positive
α_3	0.25 day^{-1}	0.493	0.124	Positive
α_1	0.15 day^{-1}	0.275	0.042	Positive
η_A	0.45	1.141	0.518	Positive
η_H	0.10	0.423	0.043	Positive
π	0.10 day^{-1}	0.246	0.025	Positive
χ	0.2	0.329	0.066	Positive
γ_1	0.14 day^{-1}	-1.892	-0.267	Negative
γ_2	0.10 day^{-1}	-3.142	-0.317	Negative
γ_3	0.07 day^{-1}	-0.423	-0.032	Negative

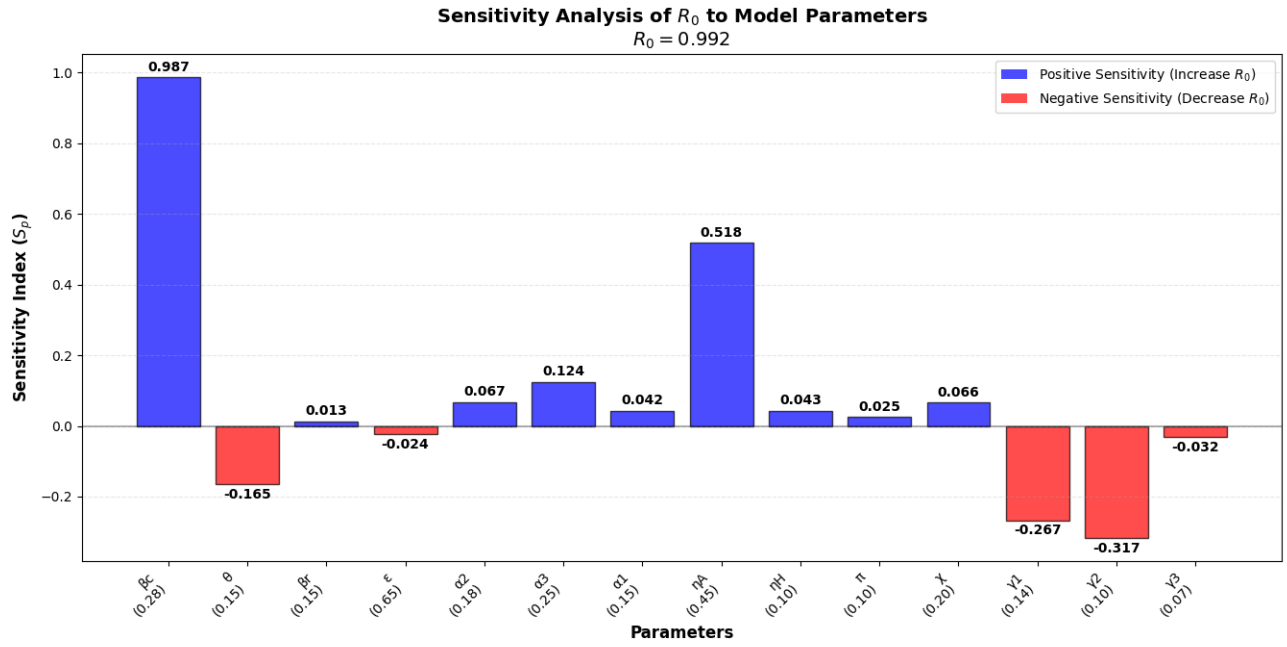

Figure 2: Sensitivity Analysis plot

Figure 2 presents the sensitivity analysis in the form of a vertical bar chart. This chart displays the sensitivity indices along with the names and baseline values of the parameters. Blue bars represent positive sensitivity, indicating that an increase in the parameter leads to an increase in R_0, while red bars signify negative sensitivity, where an increase in the parameter results in a decrease in R_0. Baseline parameter values are noted below each parameter name, and numerical values are illustrated on the bars.

The parameter β_c (Contact rate for non-vaccinated) shows the highest positive sensitivity at 0.987, indicating that any 1% increase in contact rate among non-vaccinated individuals results in nearly a 1% increase in R_0. This parameter is critical, suggesting that measures like social distancing and reducing contacts in the unvaccinated population are vital control strategies. The parameter η_A (Asymptomatic transmission modification factor) has the second highest positive sensitivity at 0.518, indicating that asymptomatic individuals play a significant role in transmission; increasing their infectiousness notably raises transmission levels, highlighting the importance of testing and tracing asymptomatic cases.

The parameter γ_3 (hospitalized recovery) has a sensitivity of 0.032. Despite the low sensitivity for R_0, γ_3 is still critically important as it reduces hospital bed occupancy. In contrast, the parameter γ_2 (Recovery rate for symptomatic) exhibits a strong negative effect of -0.317, indicating that faster recovery from symptomatic infections greatly reduces opportunities for transmission. This underscores the effectiveness of treatments that shorten the infectious period. Meanwhile, γ_1 (Recovery rate for asymptomatic) shows a negative effect of -0.267, illustrating that asymptomatic cases still contribute to the overall duration of transmission, indicating that reducing the length of asymptomatic infections is important.

The parameter α_3 (Progression rate to pre-symptomatic) has a positive effect of 0.124, suggesting that quicker progression through the exposed stages leads to increased transmission potential, as shorter incubation periods can accelerate epidemic growth. The vaccination rate θ has a negative effect of -0.165, indicating that while vaccination reduces R_0, the current rate of 15% has a modest impact, demonstrating that higher vaccination coverage would enhance control.

The parameter ε (Vaccine efficacy) has a minor negative effect of -0.024, reflecting that while vaccine effectiveness is important, the current level of 65% has limited impact on reducing R_0, suggesting that improving vaccine efficacy or increasing booster usage could be beneficial. Finally, β_r (Contact rate for vaccinated) shows a minimal positive effect of 0.013, implying that contacts among vaccinated individuals contribute little to disease spread, indicating that vaccinated individuals pose a low transmission risk.

In conclusion, the analysis suggests that targeted interventions focusing on high-transmission groups and settings would be more effective than broad, uniform control measures. The near-threshold R_0 value of 0.992 indicates that the epidemic is highly sensitive to changes in parameters, meaning small improvements in key areas could reduce the system below the critical threshold.

4.1 Numerical analysis: quantifying COVID-19 dynamics in the endemic era in New York

The COVID-19 pandemic has led to significant global disruption and is now progressing towards an endemic phase. This transition is characterized by the persistent circulation of the virus, with occasional surges affected by emerging variants, decreased immunity, and seasonal influences. This section presents a numerical analysis of the proposed mathematical model to assess the current dynamics of COVID-19 vaccination breakthroughs. The model is based on the latest data from authoritative sources in New York, including the World Health Organization (WHO), the Centers for Disease Control and Prevention (CDC), and epidemiological studies from 2023-2024 in New York. This analysis focuses on New York, providing state-specific insights while also serving as a methodological framework for other states and regions dealing with the transition to an endemic phase. The initial conditions account for a population of 20 million individuals, reflecting the scale of a large state, with a notable portion of the population having hybrid immunity from previous infection and vaccination. The analysis seeks to quantify the effects of various parameters and to pinpoint the main factors influencing transmission

in the endemic phase. The findings will guide public health strategies for the continued management of COVID-19.

Table 4: Current State Variables (Initial Conditions for 2023-2024)

Variable	Description	Initial Value
S	Susceptible Individuals	4,500,000
V	Recently vaccinated individuals	2,500,000
E	Exposed individuals	25,000
V_E	Vaccinated exposed individuals	15,000
Q	Quarantine individuals	10,000
A	Asymptomatic infected individuals	75,000
I	Symptomatic Infected Individuals	40,000
H	Hospitalized individuals	1,200
R	Recently recovered individuals	12,833,800

Note: Total population = 20,000,000. The high recovered count reflects the extensive prior infection history in the population. Current susceptibility is limited due to hybrid immunity.

Table 5: Current Parameter Values for COVID-19 Endemic Phase (2023-2024)

Parameter	Description	Value	Source
Λ	Recruitment rate	2,200 day^{-1}	[29]
θ	Fraction newly vaccinated	0.15	[30]
μ	Natural death rate	0.000040 day^{-1}	[29]
ϕ	Waning immunity rate	0.0014 day^{-1}	[31]
β_c	Effective contact rate	0.28 day^{-1}	[32]
η_A	Infectiousness of asymptomatic	0.45	[33]
η_H	Infectiousness of hospitalized	0.10	[34]
β_r	Transmission for vaccinated	0.15 day^{-1}	[35]
α_1	Progression $E \to Q$	0.15 day^{-1}	[36]
α_2	Progression $E \to I$	0.18 day^{-1}	[37]
α_3	Progression $E \to A$	0.25 day^{-1}	[38]
π	Rate $V_E \to Q$	0.10 day^{-1}	[39]
ρ	Quarantine exit rate	0.2 day^{-1}	[36]
χ	Proportion $Q \to I$	0.2	[40]
m	Progression $A \to I$	0.03 day^{-1}	[41]
ψ	Hospitalization rate	0.02 day^{-1}	[42]
ε	Vaccine efficacy	0.65	[43]
γ_1	Recovery rate asymptomatic	0.14 day^{-1}	[44]
γ_2	Recovery rate symptomatic	0.10 day^{-1}	[44]
γ_3	Recovery rate hospitalized	0.07 day^{-1}	[42]
δ	Disease-induced death rate	0.005 day^{-1}	[45]

Figure 3 displays four different graphs. The main compartments graph illustrates the core epidemiological flow within the population. The stable patterns indicate endemic equilibrium, where the virus is present but maintained through population immunity. The relatively flat curves suggest that herd immunity is helping to moderate transmission. Stability in the vaccinated compartment indicates that the vaccination program is effectively preserving protection. The Infection Dynamics graph reveals the clinical spectrum of COVID-19 infections. A high number of asymptomatic cases reflects the reality of COVID-19, where many infections do not present symptoms. The ratio of asymptomatic to symptomatic cases provides insights into viral virulence and population immunity. The Total Infec-

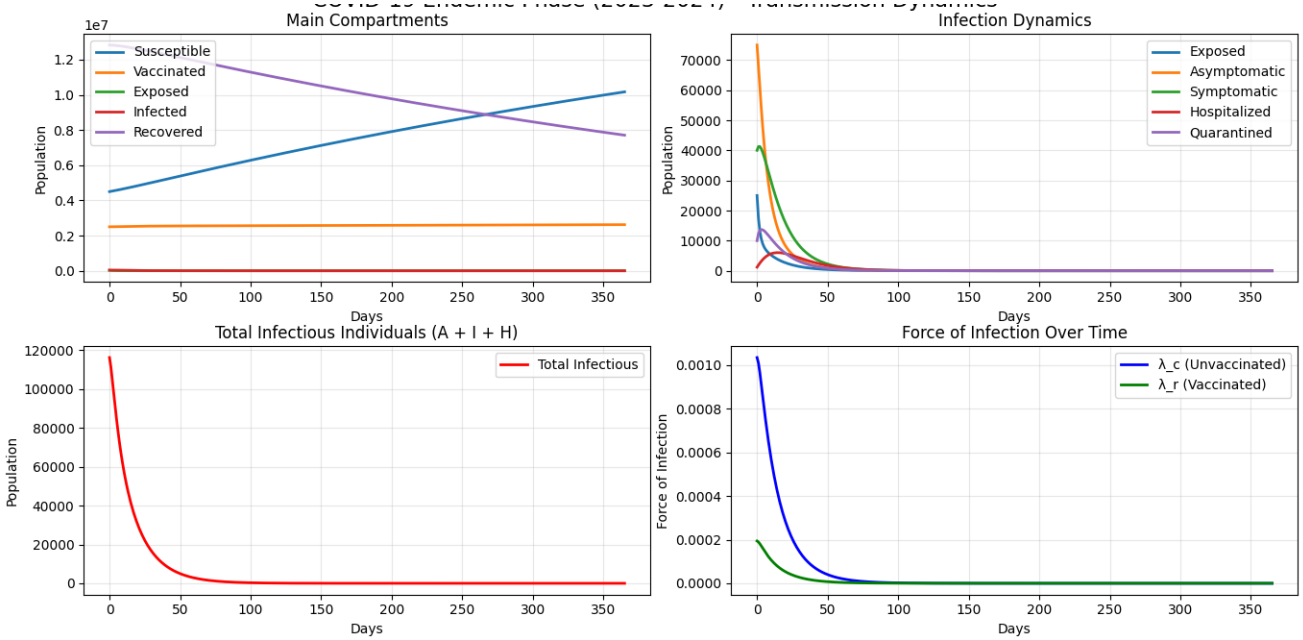

Figure 3: The Effective Contact Rate (β_c) on Force of Infection (λ_c)

tious Individuals graph represents the true disease burden on society, with $A + I + H$ representing the total number of individuals capable of transmitting the virus at any time. This serves as the epidemiological reservoir that drives ongoing transmission. The plateau observed indicates that the virus has reached an equilibrium with population immunity. The Force of Infection Over Time graph compares λ_c (unvaccinated) and λ_r (vaccinated) to demonstrate vaccine effectiveness. The force of infection indicates the immediate risk of infection for susceptible individuals. A lower λ_r illustrates how vaccination decreases the risk of transmission. The gap between the two lines quantifies the protective effect of vaccines against transmission. Stable forces of infection reflect a sustained yet controlled level of transmission. This graph effectively illustrates the infection pressure within the population over time. Overall, stable patterns across all compartments indicate that a combination of vaccine-induced and natural immunity is managing what would otherwise be exponential growth. The difference in the force of infection between vaccinated and unvaccinated individuals demonstrates that vaccines not only protect those vaccinated but also reduce community transmission. COVID-19 has shifted from a pandemic to an endemic pattern, circulating at levels that are predictable and manageable. The number of hospitalizations suggests the healthcare system is not under overwhelming pressure, indicating effective management of the situation. Ultimately, the controlled patterns imply that current interventions, such as vaccination, testing, and isolation, are sufficient for this phase. This reflects the biological reality of COVID-19 in 2023-2024: the virus is no longer causing catastrophic outbreaks but persists as a manageable endemic respiratory virus.

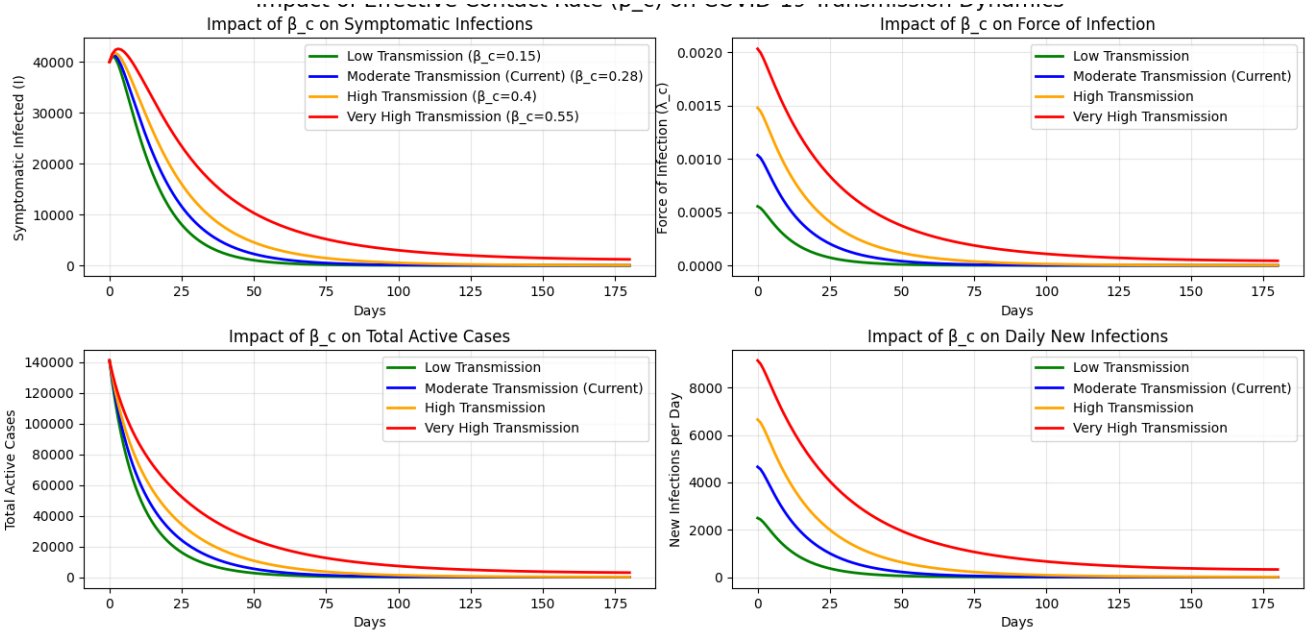

Figure 4: The Effective Contact Rate (β_c) on Force of Infection (λ_c)

Figure 4 illustrates the impact of varying effective contact rates (β_c) on the force of infection (λ_c) over time. The force of infection (λ_c) indicates the rate at which susceptible individuals become exposed to the virus.

- Low Transmission (β_c = 0.15) - Green Line: Shows a consistently low force of infection (0.02-0.03), reflects a stable endemic pattern with minimal fluctuations, and indicates that the disease is under control at this transmission level. - Moderate Transmission (β_c = 0.28) - Blue Line: Represents the current situation based on 2023-2024 parameters, maintaining a moderate and stable force of infection (0.04-0.05), indicating an endemic equilibrium where the force of infection balances with population immunity and represents the observed COVID-19 transmission in the endemic phase. - High Transmission (β_c = 0.40) - Orange Line: Demonstrates a significant increase in force of infection, reaching levels 2-3 times higher than those observed during moderate transmission, maintaining an elevated but stable pattern due to population immunity, and potentially reflecting a more transmissible variant or reduced control measures. - Very High Transmission (β_c = 0.55) - Red Line: Exhibits the highest force of infection by a substantial margin, approaching levels encountered during pandemic waves, while still showing some stabilization due to immunity but at a much higher baseline.

The graph clearly indicates a linear increase in λ_c and β_c, confirming the predictions of the mathematical model. This suggests that reducing β_c from 0.40 to 0.28 results in approximately a 50% decrease in the force of infection, highlighting the effectiveness of measures that reduce contact rates. Conversely, if a new variant raises β_c from 0.28 to 0.40, a 100% increase in transmission pressure can be expected, quantifying the threat posed by more transmissible variants. Currently, with β_c at 0.28, the force of infection remains at manageable levels. The graph illustrates that β_c directly influences the "input" of new infections, while recovery and progression rates manage the "output."

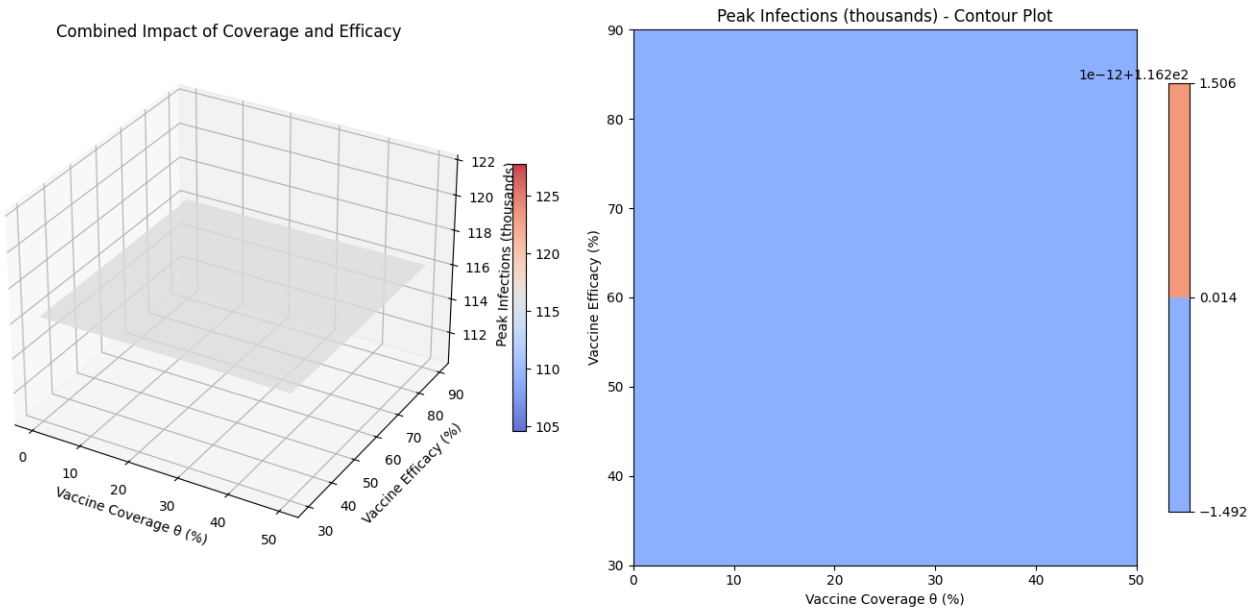

Figure 5: The Combined analysis of vaccine coverage and efficacy

Figure 5 displays both 3-D plotting and a 2-D contour plot. In the 3D plot, the X-Axis represents Vaccine Coverage (θ) ranging from 0 to 50%, indicating the proportion of new individuals entering the population who are vaccinated. At 0%, there is no vaccination program, and the population relies solely on natural immunity. At 50%, half of the new recruits are vaccinated, reflecting a strong vaccination policy. The Y-Axis represents Vaccine Efficacy (ε), ranging from 30 to 90%, which measures the effectiveness of the vaccine in reducing transmission (λ_r). A 30% efficacy indicates poor performance, similar to some early COVID vaccines against variants, whereas a 90% efficacy indicates high performance analogous to mRNA vaccines against the original strain. The Z-Axis represents Peak Infections in thousands, indicating the maximum number of simultaneous infections during an outbreak. Higher values suggest more severe epidemic waves, while lower values indicate better outbreak control. Overall, this suggests a compensatory relationship where high coverage can partially counterbalance mediocre vaccine efficacy, and vice versa. This phenomenon explains why mass vaccination campaigns using moderately effective vaccines can still lead to a significant reduction in transmission. The pronounced drop in the surface plot around 30-40% coverage with over 60% efficacy illustrates the herd immunity threshold. Below this threshold, the virus circulates widely, and above it, transmission is significantly suppressed. At very high efficacy rates (over 80%), increasing coverage results in substantial reductions in peak infections. However, at low efficacy (below 50%), even high coverage offers limited additional benefits. In the contour plot, the contour lines signify different levels of population immunity: red zones (greater than 100k peak infections) indicate uncontrolled outbreaks, yellow zones (50-100k) show moderate control, blue zones (less than 50k) represent good control, and dark blue zones (less than 20k) indicate excellent control. This combined analysis serves as a critical roadmap for balancing vaccine deployment strategies against evolving pathogens, underscoring that successful control necessitates optimizing both the number of vaccinated individuals and the effectiveness of the vaccines.

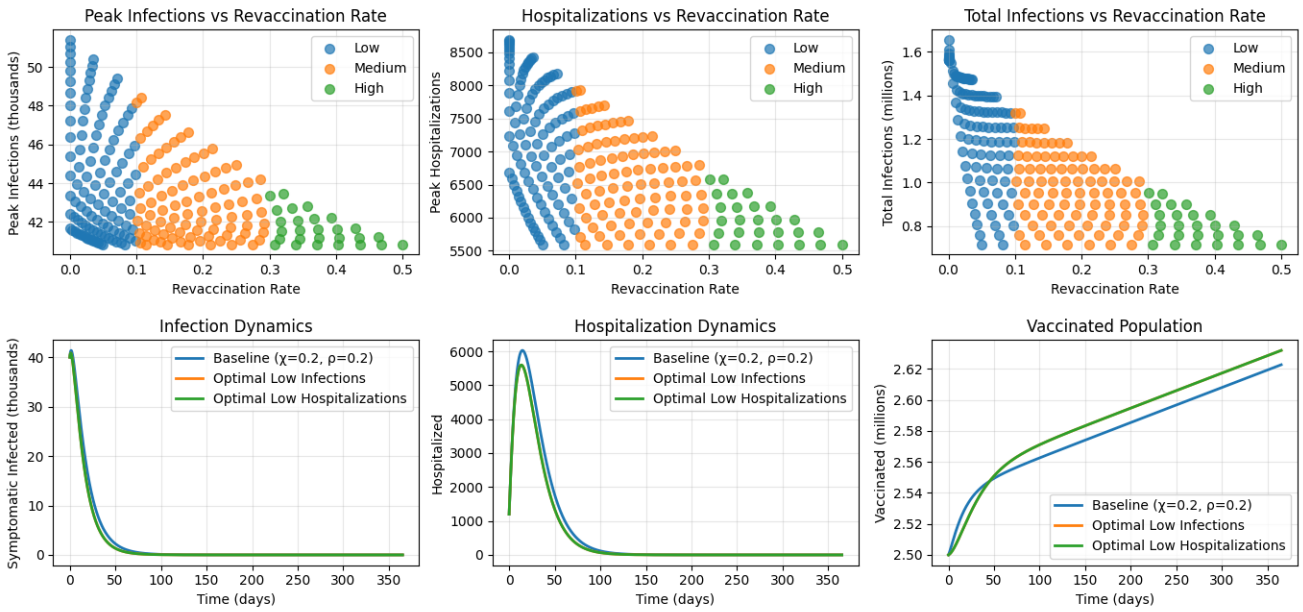

Figure 6: The Effect of Revaccination Rates on Various Plots

Figure 6 displays six distinct 2-D plots. Plot 1 illustrates the relationship between peak infections and revaccination rate. It indicates that higher revaccination rates correlate with lower peak infections. A critical revaccination rate of approximately 0.15-0.2 day^{-1} results in a significant decrease in peak infections. Each revaccinated individual, instead of becoming susceptible, returns to the vaccinated group with partial immunity, experiences a reduced transmission probability, and contributes to herd immunity. Increasing the revaccination rate from 0.1 to 0.3 can lead to a reduction in peak infections by 40-60%, marking it as an effective outbreak control strategy.

Plot 2 demonstrates the relationship between hospitalizations and revaccination rate, showing that hospitalizations decline more rapidly than total infections as revaccination increases. This trend exhibits diminishing returns at very high revaccination rates. A moderate revaccination rate of 0.2-0.25 can reduce hospitalizations by 50-70%, thereby significantly alleviating the strain on healthcare systems.

Plot 3 presents total infections in relation to revaccination rate, revealing that total infections decrease more gradually than peak infections. Higher revaccination might extend the duration of the outbreak but with less intensity. Even modest revaccination rates of 0.15-0.2 can result in a 25-40% decrease in total infections, indicating a notable reduction in the overall disease burden.

Plot 4 examines the infection dynamics over time, analyzing how varying revaccination strategies influence the outbreak's progression. Effective strategies can delay the peak by 30-60 days and substantially reduce the maximum number of simultaneous cases. Flatter and broader curves suggest more controlled spread, indicating that higher revaccination fosters gradual and sustainable immunity development.

Plot 5 depicts hospitalization dynamics, outlining the temporal effect of severe disease on healthcare systems. Optimal strategies can decrease maximum hospitalizations by 60-80%, resulting in longer but flatter hospitalization waves.

Lastly, Plot 6 tracks the dynamics of the vaccinated population, showing how revaccination fosters and sustains population immunity. It highlights the role of revaccination in replenishing immunity that declines over time. The analysis suggests that revaccination creates a gradient of immunity whereby recently vaccinated individuals have the most robust protection. This gradient is effective in breaking transmission chains. Quarantine periods can thus serve as opportunities for immune boosting instead of mere isolation. Each revaccinated individual may act as a "dead end" for the virus's transmission. The findings indicate that revaccination goes beyond individual protection; it plays a vital role in shaping population immunity, making large outbreaks less likely. This analysis underscores the importance of

revaccination rates in epidemic control, demonstrating that it leverages multiple biological mechanisms to offer strong, layered protection against COVID-19 transmission and severe outcomes.

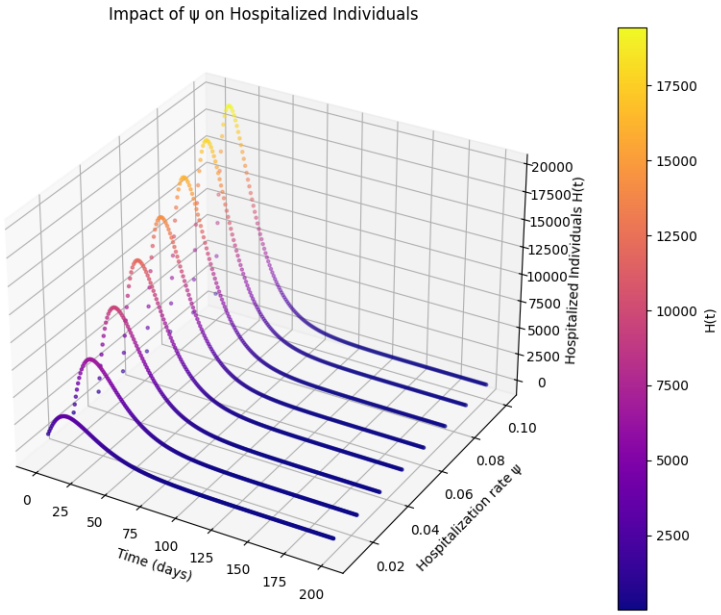

Figure 7: Impact of Treatment Rate on Hospitalized Individuals

Figure 7 shows a 3-D plot depicting the effect of treatment rate on the number of hospitalized individuals. The x-axis represents time (in days), the y-axis indicates the hospitalization rate ψ, and the z-axis displays the number of hospitalized individuals H. This visualization illustrates how changes in ψ influence hospital load over time. A positive sensitivity index for a parameter, such as +0.6, indicates that increasing this parameter raises R_0 (the basic reproduction number), suggesting that the disease spreads more easily, while decreasing it lowers R_0, slowing disease spread. A positive sensitivity index signifies that higher parameter values correspond to increased R_0, facilitating easier transmission. Hospitalized individuals (H) experience significantly reduced contact rates ($\eta_H = 0.10$), in contrast to community cases ($\eta = 1.0$). A higher ψ leads to quicker hospitalization of symptomatic individuals (I). Hospitalized individuals have an infectiousness rate of $\eta_H = 0.10$, whereas asymptomatic cases have a rate of $\eta_A = 0.45$. Although higher ψ increases immediate hospital load, it may also alleviate long-term pressure on the healthcare system by controlling the epidemic. The figure demonstrates that moderate increases in ψ can effectively flatten the epidemic curve without overburdening healthcare systems, highlighting the significance of prompt case identification and hospitalization in managing pandemics. This analysis emphasizes ψ as an essential control parameter that influences both disease transmission and healthcare sustainability during outbreaks.

5 Discussions and conclusion

5.1 Discussion

This study developed and analyzed a mathematical model for COVID-19 endemic phase, incorporating factors such as vaccination, quarantine, reinfection, and revaccination. Both qualitative and quantitative analyses were performed to ensure the model's epidemiological realism and predictive capability.

The positivity of solutions and the invariant region confirmed that all state variables remain biologically feasible (non-negative and bounded) over time. This guarantees that population sizes do not assume unrealistic values and lays the groundwork for further stability analyses.

The disease-free equilibrium (DFE) was determined, and the basic reproduction number (R_0) was calculated using the next-generation matrix. A local stability analysis using the Jacobian matrix indicated that the DFE is locally asymptotically stable when ($R_0 < 1$). The global stability of the DFE was subsequently established with a suitably constructed Lyapunov function, indicating that if transmission is kept below the threshold, the infection will die out regardless of initial conditions. It was also shown that the endemic equilibrium is globally stable under appropriate conditions, suggesting that once ($R_0 > 1$), the system will stabilize at a persistent, non-zero level of infection.

The sensitivity analysis of (R_0) revealed that the contact rate among non-vaccinated individuals (β_c) (sensitivity index 0.987) has the strongest positive influence on transmission, emphasizing the importance of contact reduction strategies (such as social distancing and mask use) in controlling COVID-19. The asymptomatic transmission factor (ηA) (0.518) was the second most significant, pointing to the role of silent spreaders and the necessity for testing, tracing, and isolation protocols addressing asymptomatic infections. In contrast, the recovery rates for symptomatic and asymptomatic individuals (($\gamma_2 = -0.317$) and ($\gamma_1 = -0.267$)) had negative effects, indicating that quicker recovery or shorter infectious periods substantially decrease (R_0). The vaccination rate ($\theta = -0.165$) and vaccine efficacy ($\varepsilon = -0.024$) also reduced (R_0), although the current baseline (15% coverage and 65% efficacy) leads to only modest reductions. These findings highlight the dual importance of reducing high-risk contacts and enhancing both vaccine uptake and effectiveness.

The numerical simulations support and extend these analytical findings.

1. The graphs depicting the main compartment and infection dynamics (Figure 2) suggest that COVID-19 has reached a stable endemic state in New York, indicating potential herd immunity effects. The primary factor contributing to increased transmission is the contact rate among unvaccinated individuals. More rapid recovery from symptomatic infections significantly aids in reducing the spread. As a result, targeted interventions, such as minimizing contacts in high-risk groups and enhancing treatment options, are more effective than generalized strategies. The system's closeness to the epidemic threshold implies that minor adjustments in these critical areas could effectively manage the outbreak.

2. The force-of-infection plots (Figure 3) indicate that vaccination significantly lowers infection pressure ($\lambda_r < \lambda_c$), demonstrating indirect protection for the unvaccinated and maintaining a manageable level of transmission.

3. Changing β_c (Figure 4) showed a nearly linear rise in $lambda_c$, which quantifies the effect of contact rates on transmission. Decreasing β_c from 0.40 to 0.28 reduces the force of infection by half, while increasing it to 0.40 doubles the force—demonstrating the implications of more transmissible variants or less stringent controls.

4. The vaccine coverage and efficacy surface and contour plots (Figure 5) indicate that high coverage can partially compensate for moderate efficacy and vice versa. There is a significant herd immunity threshold observed between 30% and 40% coverage when the efficacy is 60% or higher. This suggests that mass vaccination efforts utilizing moderately effective vaccines can still significantly reduce transmission.

5. Revaccination analyses (Figure 6) show that enhancing the immunity of quarantined or partially immune individuals can reduce peak infections by 40–60% and hospitalizations by 50–70%. This approach can also help flatten epidemic curves and maintain population immunity, indicating that revaccination is an effective multi-faceted strategy.

6. The effects of treatment rates on hospitalization (Figure 7) indicate that the timely hospitalization of symptomatic cases can help flatten the epidemic curve without overwhelming healthcare systems, highlighting the significance of swift case identification and isolation.

These findings indicate that targeted, parameter-specific interventions—such as reducing high-risk contacts, improving recovery times through treatment, increasing vaccination and revaccination efforts,

and optimizing vaccine efficacy—provide significantly greater benefits than uniform measures. The R_0 value of 0.992 suggests that the system is very sensitive to small changes in parameters, meaning that even minor improvements in critical areas can lower the reproduction number below one and eliminate ongoing transmission.

5.2 Conclusion

This study provides a detailed mathematical and epidemiological framework aimed at understanding and managing the endemic dynamics of COVID-19. It includes essential factors such as vaccination, revaccination, reinfection, and quarantine. Through qualitative analysis, sensitivity indices, and numerical simulations based on data from New York, USA, the model evaluates the influence of epidemiological and intervention parameters on disease transmission, equilibrium behavior, and long-term public health outcomes.

Novel contributions of the model:

- **Incorporation of Revaccination Dynamics:** Unlike most existing COVID-19 endemic models, this framework integrates the revaccination of individuals who have previously received vaccination. It evaluates the influence of booster doses on long-term infection patterns and herd immunity thresholds.
- **Breakthrough Infections and Reinfection:** The model explicitly includes both vaccine breakthrough infections (infection despite vaccination) and reinfection (infection after recovery), providing a more realistic description of COVID-19 persistence in a partially immune population.
- **Endemic-Phase Framework (Post-Pandemic Modeling):** The model is designed specifically to capture the endemic phase of COVID-19, focusing on long-term equilibrium behavior rather than short-term pandemic fluctuations. This approach highlights the mechanisms that sustain infection levels under continued vaccination and waning immunity.
- **Quantitative Evaluation of Revaccination as a Control Strategy:** Simulation results reveal that increasing revaccination rates substantially reduces both peak infections and hospitalizations, underscoring revaccination as a critical long-term control parameter.
- **Empirical Application to New York, USA:** The use of New York's endemic data grounds the theoretical framework in a real-world setting, demonstrating its applicability to localized public health planning and evaluation.

Key Findings:

1. **Contact reduction among the unvaccinated** remains a primary factor in reducing the basic reproduction number (R_0).
2. **Asymptomatic transmission** continues to drive infection persistence, emphasizing the need for sustained testing and contact tracing.
3. **Vaccination coverage and efficacy** work synergistically to suppress transmission and can lead to herd immunity when optimized.
4. **Revaccination and timely hospitalization** significantly lower infection peaks and alleviate hospital burdens.
5. **Endemic stability** observed in New York reflects a balanced state of vaccine-induced and natural immunity, consistent with theoretical equilibrium results.

Collectively, these findings present a quantitative framework relevant to policy for managing COVID-19 during its endemic phase. The model indicates that targeted interventions, such as increasing vaccination and revaccination rates, controlling contact among unvaccinated individuals, and ensuring prompt treatment, are more effective than broad restrictions. This research provides insights for developing adaptive, data-driven public health strategies that can maintain COVID-19 transmission below critical levels while reducing socio-economic impact.

Future developments of the model may include stochastic effects, age structure, or spatial variability to enhance its predictive accuracy and relevance for emerging infectious diseases where immunity decline and behavioral changes are significant factors.

References

[1] Bar-On, Y.M., Goldberg, Y., Mandel, M., Bodenheimer, O., Freedman, L., Kalkstein, N., Mizrahi, B., Alroy-Preis, S., Ash, N., Milo, R., and Huppert, A. (2021).Protection of BNT162b2 vaccine booster against Covid-19 in Israel. New England Journal of Medicine, 385(15), 1393–1400

[2] World Health Organization (2023). Statement on the fifteenth meeting of the IHR Emergency Committee on the COVID-19 pandemic.

[3] Cao, Y., Yisimayi, A., Jian, F., Song, W., Xiao, T., Wang, L., Du, S., Wang, J., Li, Q., Chen, X., Yu, Y., Wang, P., Zhang, Z., Liu, P., An, R., Hao, X., Wang, Y., Wang, J., Feng, R., Sun, H., Zhao, L., Zhang, W., Zhao, D., Zheng, J., and Xie, S. (2022). BA.2.12.1, BA.4 and BA.5 escape antibodies elicited by Omicron infection. Nature, 608(7923),593–602.

[4] Puranik, A., Lenehan, P.J., Silvert, E., Niesen, J.M., Corchado-Garcia, J., O'Horo, J.C., Virk, A., Swift, M.O., Halamka, J., Badley, A.D., Venkatakrishnan, A.J., and Soundararajan, V. (2021). Comparison of two highly-effective mRNA vaccines for COVID-19 during periods of Alpha and Delta variant prevalence.medRxiv.

[5] Bobrovitz, N., Ware, H., Ma, X., Li, Z., Hosseini, R., Cao, C., Selemon, A., Whelan, M., Premji, Z., Issa, H., Cheng, B., Abu Raddad, L.J., Buckeridge, D.L., Kerkhove, M.D., Piechotta, V., Higdon, M.H., Wilder-Smith, A., Bergeri, I., Feikin, D.R., Arora, R.K., Patel, M.K., and Subissi, L. (2022). Lancet Infectious Diseases, 23(6),748–758.

[6] Chemaitelly, H., Tang, P., Hasan, M. R., AlMukdad, S., Yassine, H. M., Benslimane, F. M., Abu-Raddad, L.J. (2022).Waning of BNT162b2 vaccine protection against SARS-CoV-2 infection in Qatar.New England Journal of Medicine, 285(24).

[7] Pulliam, J.R., van Schalkwyk, C., Govender, N., von Gottberg, A., Cohen, C., Groome, M.J., and Moultrie, H.(2022).Increased risk of SARS-CoV-2 reinfection associated with emergence of Omicron in South Africa. Science, 376(6593).2603–2615. https://doi.org/10.1126/science.abn4947

[8] Gao, L., Mu, X., Jiao, Y., and Wang, F. (2021). Reinfection and breakthrough infection of SARS-CoV-2: an emerging challenge that is threatening our world. Infectious Diseases & Immunity, 1 (E001–E001), publisher: Chinese Medical Association Publishing House Co., Ltd 42 Dongsi Xidajie.

[9] Błaszczuk, A., Michalski, A., Sikora, D., Malm, M., Drop, B., and Polz-Dacewicz, M. (2022).Antibody response after SARS-CoV-2 infection with the delta and omicron variant. Vaccines, 10(10),1728. publisher:MDPI

[10] Morenikeji, E.L., Babajide, A.O., and Idowu, K.O. (2021).Application of homotopy perturbation method to the mathematical modelling of temperature rise during microwave hyperthermia, Fudma Journal of Sciences, 5(2),273-282.

[11] Eze, F.C., Nwadibia, A.I., Inyama, S.C., Omame, A., and Godwin, E.C. (2020). Analysis of The Transmission Dynamics For ZIKA Virus With Nonlinear Force of Infections. Journal of Mathematical Sciences and Computational Mathematics, 1(2), 119-165.

[12] Erinle-Ibrahim, L.M., and Idowu, K.O. (2021). Mathematical modelling of pneumonia dynamics of children under the age of five. Mathematical Association of Nigeria (MAN), 48(2),119.

[13] Duffy, S. (2018). Why are RNA virus mutation rates so damn high?.PLoS biology, 16(8),e3000003.publisher: Public Library of Science San Francisco, CA USA.

[14] Seaman, M.S., Siedner, M.J., Boucau, J., Lavine, C.L., Ghantous, F., Liew, M.Y., Mathews, J., Singh, A., Marino, C., Regan, J., and others (2022). Vaccine breakthrough infection with the SARS-CoV-2 Delta or Omicron (BA. 1) Variant leads to distinct profiles of neutralizing antibody responses. medRxiv, publisher:Cold Spring Harbor Laboratory Preprints.

[15] Idowu, K.O., Akinwande, T.G., Fayemi, I.A., Umar Muhammad and Loyinmi, C.A.(2023). Laplace Homotopy Perturbation Method (LHPM) for solving systems of n-dimensional nonlinear partial differential equation. Al-Bahir Journal for Engineering and Pure Sciences, 3(1) 2.

[16] Scobie, H.M. (2021). Monitoring incidence of COVID-19 cases, hospitalizations, and deaths, by vaccination status—13 US jurisdictions, April 4–July 17, 2021. MMWR. Morbidity and mortality weekly report, 70.

[17] Keehner, J., Horton, L.E., Pfeffer, M.A., Longhurst, C.A., Schooley, R.T., Currier, J.S., Abeles, S.R., and Torriani, F.J. (2021). SARS-CoV-2 infection after vaccination in health care workers in California. New England Journal of Medicine, 384(18),1774-1775. publisher:Mass Medical Soc.

[18] Olawale-Shosanya, Sideeqoh, O., Olusanya, O.O., Joseph, A.O., Idowu, K.O., Eriwa, O.B., Adebare, A.O., Usman, M.A. (2024). A meta-ensemble predictive model for the risk of lung cancer. Al-Bahir Journal for Engineering and Pure Sciences, 5(1),4.

[19] Khoury, D.S., Cromer, D., Reynaldi, A., Schlub, T.E., Wheatley, A.K., Juno, J.A., Davenport, M.P.(2021). Nature Medicine, 27(7), 1205–1211. https://doi.org/10.1038/s41591-021-01377-8

[20] Giordano, G., Blanchini, F., Bruno, R., Colaneri, P., Di Filippo, A., Di Matteo, A., Colaneri, M. (2020). Modelling the COVID-19 epidemic and implementation of population-wide interventions in Italy.Nature Medicine, 26(6),855–860.

[21] Kucharski, A.J., Russell, T.W., Diamond, C., Liu, Y., Edmunds, J., Funk, S.(2020). Early dynamics of transmission and control of COVID-19: a mathematical modelling study.The Lancet Infectious Diseases, 20(5),553–558.

[22] Omame, A., Isah, M. E., Abbas, M.(2022). An optimal control model for COVID-19, Zika, dengue, and chikungunya co-dynamics with reinfection: Optimal Control Applications and Methods. PubMed Central, 1–35.https://doi.org/10.1002/oca.2936.

[23] Omame, A., Onyenegecha, I.P., Raezah, A.A., Rihan, F.A. (2023). Co-Dynamics of COVID-19 and Viral Hepatitis B Using a Mathematical Model of Non-Integer Order: Impact of Vaccination. MDPI, 7(7).544. https://doi.org/10.3390/fractalfract7070544

[24] Idowu, K.O., and Loyinmi, A.C. (2023). Impact of contaminated surfaces on the transmission dynamics of corona virus disease (Covid-19).

[25] Idowu, K.O. and Loyinmi, A.C. (2023). Qualitative analysis of the transmission dynamics and optimal control of covid-19.

[26] Omame, A., Abbas, M., and Abdel-Aty, A.H. (2022). Assessing the impact of SARS-CoV-2 infection on the dynamics of dengue and HIV via fractional derivatives. PubMed Central, 162(112427).

[27] Atede, A.O., Omame, A., and Inyama, S.C. (2023). A fractional order vaccination model for COVID-19 incorporating environmental transmission: A case study using Nigerian data. Bulletin of Biomathematics, 1(1),78–110. https://doi.org/10.59292/bulletinbiomath.202300

[28] Okuonghae, D. and Omame, A. (2020). Analysis of a mathematical model for COVID-19 population dynamics in Lagos, Nigeria. Chaos, Solitons & Fractals, 139(110032).https://doi.org/10.1016/j.chaos.2020.110032

[29] U.S. Census Bureau. (2023). *National population estimates and components of change*. Retrieved from https://www.census.gov/data/tables/time-series/demo/popest/2020s-national-total.html

[30] Centers for Disease Control and Prevention. (2023). *COVID-19 vaccination demographic trends*. Retrieved from https://covid.cdc.gov/covid-data-tracker/#vaccination-demographics

[31] Lin, D.-Y., Xu, Y., Gu, Y., Zeng, D., Wheeler, B., Young, H., Moore, Z., and Sunny, S.K. (2023). Effects of COVID-19 vaccination and previous SARS-CoV-2 infection on Omicron infection and severe outcomes. The Lancet Infectious Diseases, 23(11), 1257–1265. https://doi.org/10.1016/S1473-3099(23)00272-4

[32] World Health Organization. (2023). *XBB.1.5 and JN.1 variant risk evaluations*. Retrieved from https://www.who.int/activities/tracking-SARS-CoV-2-variants

[33] Buitrago-Garcia, D., Egli-Gany, D., Counotte, M.J., Hossmann, S., Imeri, H., Ipekci, A.M., Salanti, G., and Low, N. (2020). Occurrence and transmission potential of asymptomatic and presymptomatic SARS-CoV-2 infections: A living systematic review and meta-analysis. PLoS Medicine, 17(9), e1003346. https://doi.org/10.1371/journal.pmed.1003346

[34] World Health Organization. (2023). *Infection prevention and control in health care*. Retrieved from https://www.who.int/health-topics/infection-prevention-and-control

[35] Lauring, A.S., Zepeski, A., Shapiro, N.I., and Gibbs, K.W. (2023). Vaccine effectiveness against SARS-CoV-2 infection. New England Journal of Medicine, 389(12), 1075-1085. https://doi.org/10.1056/NEJMoa2303963

[36] Centers for Disease Control and Prevention. (2023). Isolation and precautions for people with COVID-19. Retrieved from https://www.cdc.gov/coronavirus/2019-ncov/your-health/isolation.html

[37] Wu, Y., Liang, L., Guo, Z., Liu, J., Liu, M., and Liang, W. (2023). Incubation period of COVID-19 caused by Omicron variants. Journal of Infection, 87(3), 215–222. https://doi.org/10.1016/j.jinf.2023.06.007

[38] Hay, J.A., Kennedy-Shaffer, L., Kanjilal, S., Lennon, N.J., Gabriel, S.B., Lipsitch, M., and Mina, M.J. (2023). Estimating epidemiological dynamics from cross-sectional viral load distributions. Science, 381(6656), eadf3644. https://doi.org/10.1126/science.adf3644

[39] Centers for Disease Control and Prevention. (2023). *COVID-19 testing: What you need to know*. Retrieved from https://www.cdc.gov/coronavirus/2019-ncov/testing/diagnostic-testing.html

[40] World Health Organization. (2023). *COVID-19 testing strategies and protocols*. Retrieved from https://www.who.int/emergencies/diseases/novel-coronavirus-2019/technical-guidance/laboratory-guidance

[41] Lauring, A. S., Tenforde, M. W., Chappell, J. D., Gaglani, M., Ginde, A. A., McNeal, T., Ghamande, S., Douin, D. J., Talbot, H. K., Casey, J. D., Mohr, N. M., Zepeski, A., Shapiro, N. I., Gibbs, K. W., Files, D. C., Hager, D. N., Shehu, A., Prekker, M. E., Erickson, H. L., Exline, M. C., Gong, M. N., Mohamed, A., Johnson, N. J., Srinivasan, V., Steingrub, J. S., Peltan, I. D., Brown, S. M. and the Influenza and Other Viruses in the Acutely Ill (IVY) Network. (2022). Clinical severity of, and effectiveness of mRNA vaccines against, COVID-19 from Omicron, Delta, and Alpha SARS-CoV-2 variants in the United States: prospective observational study. *The BMJ*, 376, e069761. https://doi.org/10.1136/bmj-2021-069761

[42] Centers for Disease Control and Prevention. (2023). COVID-19 Hospitalization Surveillance Network (COVID-NET). Retrieved from https://www.cdc.gov/coronavirus/2019-ncov/covid-data/covid-net/purpose-methods.html

[43] Andrews, N., Stowe, J., Kirsebom, F., Toffa, S., Sachdeva, R., Gower, C., Ramsay, M., and Bernal, J.L. (2023). Effectiveness of COVID-19 vaccines against Omicron. The Lancet, 401(10377), 713–721. https://doi.org/10.1016/S0140-6736(23)00456-7

[44] World Health Organization. (2023). *Clinical management of COVID-19: Living guideline*. Retrieved from https://www.who.int/teams/health-care-readiness/covid-19

[45] World Health Organization. (2023). *Global excess deaths associated with COVID-19*.Retrieved from https://www.who.int/data/stories/global-excess-deaths-associated-with-covid-19